NISTIR 5266

In Situ Burning of Oil Spills: Mesoscale Experiments

William D. Walton

Building and Fire Research Laboratory
Gaithersburg, Maryland 20899

United States Department of Commerce
Technology Administration
National Institute of Standards and Technology

NISTIR 5266

In Situ Burning of Oil Spills: Mesoscale Experiments

William D. Walton

November 1993

Building and Fire Research Laboratory
National Institute of Standards and Technology
Gaithersburg, MD 20899

U.S. Department of Commerce
Ronald H. Brown, *Secretary*
Technology Administration
Mary L. Good, *Under Secretary for Technology*
National Institute of Standards and Technology
Arati Prabhakar, *Director*

Prepared for:
U.S. Department of Interior
Bruce Babbitt, *Secretary*
Minerals Management Service
Technology Assessment and Research Branch
Herndon, VA 22070

LIST OF TABLES

LIST OF FIGURES

Page

In Situ Burning of Oil Spills: Mesoscale Experiments

William D. Walton
Building and Fire Research Laboratory,
U.S. National Institute of Standards and Technology

ABSTRACT

In 1991 a series of 14 mesoscale fire experiments were performed to measure the burning characteristics of crude oil on salt water. These oil burns in a pan ranged in size from 6 m square to 15 m square. Results of the measurements for burning rate, oil temperature, water temperature, smoke particle size distribution, smoke plume trajectory, and smoke particulate yield are provided. The burning rate as indicated by the regression rate of the oil surface was found to be 0.055 ± 0.005 mm/s and smoke particulate yields were found to be approximately 0.13 of the oil burned on a mass basis.

Key words: burning rate, crude oil, fire tests, heat release rate, oil spills, particle size distribution, plumes, pool fires, smoke yield, water sprays

1.0 INTRODUCTION

Recent major crude oil spills such as the Exxon Valdez spill in Prince William Sound Alaska on March 24, 1989 have demonstrated the difficulty and expense in mitigating large crude oil spills at sea. Crude oil spills at sea are one of the most difficult petroleum product spills to mitigate. Crude oil does not dissipate as rapidly as light refined products such as gasoline but it disperses far more quickly than the heaver refined products like asphalt. Some crude oils exhibit a tendency to form oil/water emulsions which generally complicates the mitigation process. Crude oil spills at sea must be mitigated rapidly to prevent damage to the marine environment. The natural evaporation of the oil along with available mitigation techniques such as mechanical recovery, the use of dispersants, and bioremediation have not proved entirely successful in the mitigation of large crude oil spills at sea. In situ burning of crude oil spills has been proposed as a technique which, under certain circumstances, can supplement other available mitigation techniques.

In situ burning of spilled oil has distinct advantages over other countermeasures. It offers the potential to convert rapidly large quantities of oil into its primary combustion products, carbon dioxide and water, with a small percentage of other unburned and residue byproducts. Burning of spilled oil from the water surface before it spreads reduces the chances of shoreline contamination and damage to biota. In situ burning requires minimal equipment and less labor than other techniques. It can be applied in areas where many other methods cannot due to lack of response infra-structure and/or lack of alternatives. Oil spills amongst ice and on ice are examples of situations where practical alternatives to burning are very limited. Because the oil is converted to gaseous products of combustion by burning, the need for physical collection, storage, and transport of recovered fluids is reduced to the few percent of the original spill volume that remains as residue after burning. It is recognized that in situ burning of crude oil spills changes the impact of the spill on the environment. In order for decision makers to assess the appropriateness of in situ burning, information comparing the impact of burning to other mitigation strategies must be made available.

Burning, once regarded as a method of last resort, is now, in some regions, one of the first response methods being considered by authorities in the event of a spill. Intentional in situ burning was used on a very limited basis in the Exxon Valdez spill[1] and in two diesel fuel spills[2]. Although it is possible in some cases to simply ignite a crude oil spill, frequently it is safer and far more efficient to corral quantities of oil and burn it in a controlled fashion. The generally accepted technique for accomplishing this is to use specially designed fire proof oil containment boom. The boom is tethered to a tow vessel at either end with a length of line and towed slowly forming the boom into a horseshoe shape. A schematic of the towed fire boom is shown in figure 1. Using the towed boom, the vessel operators corral a quantity of the spilled crude oil, which the towing action concentrates at the closed end of the boom. Experiments have shown that a minimum oil depth of approximately 3 mm is required for ignition and sustained burning[3]. When the corralled oil has been towed to a safe location for the burn, the oil is ignited by one of a number of available methods such as floating an ignitor from one of the tow vessels. The tow vessels continue to slowly tow the boom as the oil burns which concentrates the decreasing quantity of oil. When the burning ceases the remaining residue is mechanically recovered.

Burning oil spills produces a visible smoke plume containing smoke particulate and other products of combustion which may persist for many kilometers from the burn. This fact gives rise to public health concerns, related to the chemical content of the smoke plume and the downwind deposition of particulate, which need to be answered. Air quality is also affected by evaporation of large oil spills that are not burned. Volatile organic compounds (VOC) including benzene, toluene, and xylene and polycyclic aromatic hydrocarbons (PAH) are found in the air downwind of an evaporating crude oil spill. Laboratory

measurements are useful to determine the types of chemical compounds that are expected from large oil spill burns or the evaporation of the spill. To determine the rate of emissions and the transport of the chemical compounds from a burning or evaporating spill, mesoscale experiments have been conducted outdoors using a 15 m square pan. In these experiments a layer of crude oil was discharged onto the surface of a salt water pool. The local air quality during evaporation and burning of the oil was measured.

The Building and Fire Research Laboratory (BFRL) at the National Institute of Standards and Technology (NIST) has conducted research related to assessment of the capabilities of in situ burning as an oil spill response method. This work has been funded jointly by the Minerals Management Service (MMS), the U.S. Coast Guard (USCG), and the American Petroleum Institute (API). This research has focused on (a) examining the burning characteristics of crude oil fires on water, (b) the fraction of oil in a spill that can be consumed by in situ burning, (c) the characteristics of the residual oil, (d) the characteristics of the combustion products, and (e) the fate of particulate material carried in the smoke plume. Information from both laboratory and mesoscale crude oil burns has contributed significantly to understanding the impact of oil spill burning.

A key to gaining widespread acceptance of burning as a spill response method is the demonstration that the results obtained at laboratory scale and mesoscale tests can be duplicated under simulated operational conditions during at sea burns. In 1991, NIST organized and conducted a series of mesoscale burns of crude oil on salt water at the United States Coast Guard facility on Little Sand Island in Mobile Bay Alabama, in cooperation with USCG, Environment Canada, U.S. Environmental Protection Agency-Environmental Response Team (EPA-ERT), and the U.S. National Oceanic and Atmospheric Administration (NOAA) under funding from MMS, API, and USCG. These burns were conducted in a 15 meter square burn pan constructed specifically for oil spill burning. The large pan burns were designed to be of a scale comparable to that proposed for using burning to mitigate an actual open ocean crude oil spill. Measurements in the mesoscale burns included oil burning rate, burn consumption efficiency, oil and water temperatures, thermal radiation, smoke yield, plume trajectory, smoke deposition, and analysis of the oil, smoke and burn residue.

2.0 BACKGROUND

In 1985, the Center for Fire Research (CFR), now the Building and Fire Research Laboratory (BFRL), at the U.S. National Institute of Standards and Technology (NIST) began studies of oil spill combustion under support from the Minerals Management Service (MMS) of the U.S. Department of the Interior. This work sought to quantify the processes involved in oil spill combustion on open waters and in water filled channels formed in broken ice and included measurements of smoke production and prediction of smoke dispersal. Technical support from Environment Canada allowed the study to be broadened to include chemical analysis of the oil, oil residue, and oil smoke.

At the beginning of this research program it had already been demonstrated by other investigators that burning was an efficient means of removing crude oil from the surface of the water under a variety of conditions. Experimental burns of oil in ice leads (channels of water through ice) conducted by Brown and Goodman [4] and Smith and Diaz [5] showed that 50% to 90% of an oil spill could be removed by burning. In tests in which oil pools were free to spread during burning, Buist and Twardus [6] report consumptions of 70% to 90%. The focus of the research program at NIST was to quantify the combustion process and in particular measure properties of the smoke from the crude oil fires.

In the first year of the study [7], the burning process was studied at two pool diameters, 0.6 m and 1.2 m. The emission rate, size distribution, and specific extinction coefficient (relative blackness) were measured for the smoke produced by the fires. The structure of the smoke agglomerates was examined by electron

microscopy. The burn residue left on the water by natural quenching of the combustion was analyzed and found to be depleted of short chain alkanes and cycloalkanes when compared with the fresh crude oil. A calculation of the induced air flow into a distribution of pool fires simulating the simultaneous burning of oil in many separate ice leads was performed to demonstrate the magnitude of the fire induced wind.

In the second year [8], extensive measurements of the polycyclic aromatic hydrocarbon (PAH) content of the crude oil and the smoke was performed in cooperation with Environment Canada. Measurements showed that about 10% of the crude oil was converted to smoke in the combustion process. A methodology was developed with which the down wind dispersal of smoke generated by one or more oil spill fires in close proximity may be predicted.

In the third year [9], smoke emission was measured during the burning of oil layers thin enough to cause boiling in the supporting water layer. Under these conditions both smoke emission and the PAH content of in the smoke was reduced compared to burning of thicker layers. Measurements of the optical properties and sedimentation velocities for aged and diluted smoke samples were performed. These characteristics are important in estimating smoke properties downwind of the oil spill fire. Analysis of smoke dispersal in the atmosphere were continued by formulating a model for smoke particle settling time which is directly related to soot deposition on the ground remote from the combustion site.

In the fourth year [10], measurements focussed on the determination of the agglomeration rate for smoke particles at both ambient temperature conditions, which corresponds to the cooler, diluted smoke in the plume, and at a temperature around 100 °C, which corresponds to the temperature several flame heights above the fire. Development of the plume dynamics model continued with a formulation in terms of buoyancy induced vortex trajectories (which represent the large scale plume turbulence) so that the agglomeration rate inferred from the laboratory measurements could be incorporated in the plume model. In the laboratory study, the agglomerate size was observed to increase with holding time in the aging/dilution collection chamber, while in a steady state plume model, the agglomerate size will increase with downwind position along the plume.

In the fifth year [11], preparations began for the mesoscale burns to be conducted in cooperation with the USCG at their Fire and Safety Test Detachment in Mobile, Alabama. Preparation involved the development of new instrumentation to perform measurement of combustion characteristics and smoke emissions from large crude oil pan fires up to 15 meters in diameter. Many methods of transporting instrument packages into the smoke plume were investigated during the year. Testing indicated that the best method was tethered mini-blimps. Efforts in the calculation of smoke plume trajectory were concentrated on developing models capable of predicting the "footprint" of soot particle deposition downwind of a burn.

In the sixth year [12,13], measurements with the newly developed instrumentation on large oil fires from 3 meters in diameter at the Fire Research Institute in Japan, to 15 meters diameter at both the Navy Fire Fighter Training facility in Norfolk, Virginia, and the mesoscale burns in Mobile were completed. The initial two- and three-dimensional calculations of smoke particulate transport were completed.

In the seventh year [14], the research program was concentrated on analysis of the data from the 1991 mesoscale experiments. The initial results were the major burning characteristics of mass loss rate and fraction of the oil burned that was emitted as particulate. Additional laboratory measurements of smoke yield were performed with the identical oil used in the mesoscale experiments to examine the effect of scaling. Results of the mesoscale measurements for burning rate and smoke emissions were compared to those from smaller scale burns conducted both in the U.S. and in Japan. Calculations of the smoke plume trajectory and downwind particulate deposition at ground level were completed. Predictions of

smoke plume trajectory and particulate deposition at ground level from the Large Eddy Simulation (LES) model developed as part of this research effort were found to be different from those predicted by the EPA approved SCREEN model, however there is no data available to verify either prediction. LES is a steady-state three-dimensional calculation of smoke plume trajectory and smoke particulate deposition based on a mixed finite difference and Lagrangian particle tracking method.

3.0 TEST CONFIGURATION AND INSTRUMENTATION

The mesoscale burns of crude oil were carried out under the direction of NIST at the United States Coast Guard Fire and Safety Test Detachment facility on Little Sand Island in Mobile Bay Alabama. Little Sand Island is approximately 0.2 km^2 in size and includes three decommissioned ships docked in a lagoon. The ships and facilities on the island have been used for a wide variety of full-scale marine fire tests. Figure 2 is a photograph of a burn in progress, and figure 3 is a plan view of the portion of the island used for the oil spill burns.

The burns were conducted in a nominal 15 m square steel burn pan constructed specifically for oil spill burning. The burn pan was 0.61 m deep and was constructed with two perimeter walls approximately 1.2 m apart forming an inner and outer area of the pan. The base of the pan was located on ground level. The inside dimensions of the inner area of the pan were 15.2 m by 15.2 m. The two perimeter walls were connected with baffles and the space between the walls, which formed the outer area of the pan, was filled with water from Mobile Bay during the burns. The inner area of the pan was filled with approximately 0.5 m of bay water and the crude oil was added on top of the water.

The crude oil used in the mesoscale burns was obtained from an oil storage facility in Louisiana. The oil originated from wells in the Louisiana area and is thus referred to as Louisiana crude oil. Properties of the oil, as measured by independent oil testing laboratories, are given in table 1.

Three different primary burn areas were used in the series. These areas consisted of the full inner pan with an area of 231 m^2 and partial pan areas of 114 m^2 and 37.2 m^2. The partial pan areas were achieved by partitioning the northwest corner of the inner pan with timbers covered with sheet steel.

A total of 14 mesoscale burns were conducted. These included two preliminary burns which were used to test instrumentation and procedures, 8 burns to examine the effect of burn area, and 4 burns to examine special conditions. The special conditions examined included the use of a fire resistant boom, the effect of water spray on smoke emissions and the effect of oil aging on burning. Table 2 gives the size and areas for the mesoscale burns. An effective diameter was calculated for each of the rectangular burn areas. The effective diameter is the diameter of circle with the same area as the rectangular burn area used.

3.1 Ground Based Instrumentation

The fixed position instrumentation in and around the burn pan consisted of thermocouples in the pan and a manometer to measure the liquid level in the pan.

An array of 13 1.3 mm diameter, shielded type K thermocouples was located vertically in the pan. The thermocouple array was located 2.4 m from the north side and 2.9 m from the west side of the inner wall of the pan. The thermocouple array was designed specifically to withstand the oil spill burning environment and consisted of a vertical stainless steel tube with the shielded thermocouples protruding horizontally from the tube. The vertical spacing of the thermocouples and the vertical location with respect to the fuel surface varied with each burn and is reported with the data for the burns. The base of the vertical tube was connected to a horizontal pipe which penetrated the double perimeter walls of the

pan and terminated underground. Lead wires were routed through the horizontal pipe and underground to an instrumentation building approximately 50 m from the pan. Data from the thermocouples were recorded on a computerized data acquisition system every 3 seconds.

A vertical manometer calibrated for water was used to measure the equivalent water level in the pan during the burns. Since the oil and the water in the pan have different densities, a correction must be applied to determine the thickness of the oil layer during the burn. A copper tube was connected to the inner pan water fill pipe on the pan side of the shutoff valve. The tube was run underground to the instrumentation building and connected to a liquid manometer. The liquid level in the manometer was video taped during the pan fill and burn. The equivalent water level in the pan as a function of time was obtained from the video tape record.

A portable array of 8 - 0.5 mm diameter bare-bead thermocouples 76 mm apart was used to determine the temperature of the water in the inner pan at two locations on opposite sides of the pan before and after the burns.

The ground based measurements consisted of both real time measurements and samples collected for laboratory measurement. The real time measurements made both up- and downwind of the fire included total particulates and carbon dioxide, and sulfur dioxide concentrations. Filter samples were collected both upwind and downwind of the fire and analyzed in the laboratory for PAH and VOC concentrations. Samples of the fresh oil before the burn, oil residue after the burn, and water in the burn pan after the burn were analyzed in the laboratory for PAH concentration. A detailed discussion of the ground based measurements can be found in reference [15].

3.2 Instrumentation Suspended From Tether Mini-Blimps

Airborne samples were collected for both laboratory analysis and analysis on the ground immediately following the burns. The sampling packages were suspended approximately 60 m below a 5.6 m long 2.3 m diameter tethered helium filled miniblimp. The miniblimp was positioned downwind from the fire with the sampling package centered in the smoke plume. The elevation and downwind position of the sampling package varied with each burn as a function of the plume position. Typically, sampling packages remained in the plume for 600 seconds which permitted an adequate sample to be collected and allowed the natural fluctuations in the plume to be averaged. Since the lift capacity of the miniblimp was limited, in general only a single sampling package could be deployed at a time. In some cases, where the burn was of sufficient duration, two packages were deployed sequentially.

The sampling packages consisted of battery powered pumps which drew samples through filters and discharged a portion of the gas into a collection bag. Filter samples were analyzed in the laboratory for PAH and VOC concentrations.[15] Particulate size distribution was measured using a cascade impactor. In addition, smoke particulate was collected on a thermophoretic transmission electron microscope grid (TEM grid) and analyzed using a transmission electron microscope to determine particle shape. Table 3 gives a list of the airborne samples taken during the mesoscale burns.

3.3 Weather Instrumentation

Measurements of atmospheric conditions were made with both ground based and airborne weather stations. The ground based station was located approximately 50 m to the west of the burn pan and 3 m above the ground. The station consisted of a thermistor to measure temperature, a propeller on vane anemometer to measure wind direction and speed and a capacitive relative humidity sensor. Atmospheric data from the ground based weather station were recorded every 120 s with a computerized data acquisition system.

The airborne weather station was located approximately 50 m from the pan near the ground station and was positioned for each burn to be well away from the fire plume. The airborne weather station consisted of a thermistor to measure temperature, a cup anemometer to measure wind speed, an electronic compass to measure wind direction, and a pressure transducer to measure barometric pressure. The airborne weather station was connected to a helium filled miniblimp which was tethered approximately 50 m above the ground during the fires. Data from the airborne weather station were transmitted via radio to a ground based computerized data collection system every 20 s.

4.0 EXPERIMENTAL PROCEDURE

Prior to conducting a mesoscale burn, the burn size was selected and for partial pan burns the timber partitions were positioned at the appropriate location. Water was pumped into the outer pan so that the water level was nearly to the top of the pan and water was pumped into the inner pan so that the water surface level was approximately 110 mm below the top of the pan. The distance from a reference point at the top of the pan to the surface of the water in the inner pan was measured and recorded. The temperature profile of the water in the inner pan was measured at two locations on opposite sides of the pan.

The crude oil was stored on a barge which was brought to the site prior to a burn. Oil was pumped through a flexible hose from the barge through the underground piping system and into the pan. The approximate quantity of oil delivered to the pan was monitored with an in-line flow meter. When the quantity of oil delivered to the pan approached the desired quantity, compressed air was pumped from the barge to purge the flexible hose. The barge was then disconnected from the flexible hose and the barge departed the site. The distance from the surface of the oil to the fixed reference point at the top of the pan was recorded and an oil sample was taken. The fixed position and ground based instrumentation and data recording were started and the oil was easily ignited with an extended propane torch. Video cameras were used to record the burn.

When the flames were no longer visible, the temperature profile of the water in the inner pan was measured at two locations on opposite sides of the pan. The distance from the surface of the water/oil residue to the fixed reference point at the top of the pan was recorded and a burn residue sample was taken. The residue was collected with absorbent material and placed in drums for disposal. The quantity of residue was estimated from the volume of the drums filled taking into account the absorbent material and water collected. After four of the burns (5/30, 5/31, 6/3, and 6/5), there was a greater quantity of residue than could be readily collected in two or three drums. It is estimated that there was two to three times the quantity of residue found in the earlier burns due to variations in the extinction process. In these later cases after the residue had cooled, a small quantity of diesel fuel was poured on the residue and the diesel and burn residue mixture was ignited. This procedure was repeated up to three times until the residue had been reduced to a manageable quantity. The residue was then collected and measured.

The water spray system used in burn 5/22 was designed by Alaska Clean Seas[1] to examine the effect of water spray on smoke production. Twelve nozzles which produced an umbrella like spray pattern were located approximately 1 m above the fuel surface. Bay water was pumped to the nozzles starting 83 seconds after ignition with a nozzle pressure of 34 kPa. At 373 s after ignition the pressure was increased to 69 kPa, at 507 s the valve to the spray system was closed and the spray terminated at 540 s.

---

[1] Certain commercial equipment, instruments, materials, or methods are identified in this paper in order to specify the experimental procedure adequately. Such identification is not intended to imply recommendation or endorsement by the National Institute of Standards and Technology, nor is it intended to imply that the materials or methods used are necessarily the best available for the purpose.

For the oil aging burn 5/29 the oil was pumped in the pan at 0812 hours local time and the burn started at 1627 hours local time. The oil remained on the surface of the pan for a total of approximately 29700 s prior to ignition. The analysis of the oil aging measurements can be found in reference [16].

5.0 METEOROLOGICAL DATA

Table 4 gives a summary of the meteorological conditions measured during each of the burns. The values in the table are averages over the time from ignition to extinction. Wind directions are the direction from which the wind originates with 0° being north. Although the measurements were taken at a single ground and single airborne location and there was some variation in the meteorological conditions during the burns, the burns were of relatively short duration and the averages are representative of the actual conditions. Before and after the burns, profiles of the meteorological conditions were made with the airborne weather station up to an elevation of 100 m. The profiles showed the meteorological conditions to be generally uniform above 20 m.

6.0 EFFECTIVE HEAT OF COMBUSTION

Heat is released in all combustion (oxidation) reactions. The amount of heat released per unit quantity of fuel oxidized is defined as the heat of combustion. Heat of combustion is normally determined in an ASTM D 240 oxygen bomb calorimeter, in which a known mass of fuel is burnt completely in an atmosphere of pure oxygen. In fires, however, incomplete combustion occurs resulting in the formation of carbon monoxide, smoke particles, and other incomplete combustion products. The amount of heat actually released from the fire divided by the amount of fuel burned is termed the effective heat of combustion. The Cone Calorimeter was used to determine the effective heat of combustion for the crude oil and evaluate smoke yield using three different measurement methods. The Cone Calorimeter, shown in figure 4, is more formally known as Standard Test Method for Heat and Visible Smoke Release Rates for Materials and Products Using an Oxygen Consumption Calorimeter [17]. The name of the apparatus, Cone Calorimeter, is derived from the shape of the heater used to irradiate samples. The heater coils are formed along the inner surface of a truncated cone. By imposing additional thermal radiation on the 0.085 m diameter sample of oil on water in a round container, the sample is made to burn as if it were in the middle of a larger fire. The major material flammability characteristics can be evaluated using this laboratory apparatus. These include: rate of heat release, effective heat of combustion, total heat release, ignitibility, mass loss rate, smoke specific extinction area, and yields of various gaseous species and particulate. The heat release and mass loss rates for the Louisiana oil were measured in the Cone Calorimeter, and the effective heat of combustion was determined to be 41900 kJ/kg. This effective heat of combustion was used in conjunction with the mass loss data for the mesoscale burns to determine the heat release rate of those burns.

The data from the Cone Calorimeter can also be used to determine the heat of gasification (L_v) which is the heat required to produce volatiles. The burning rate and heat of gasification are related by[18]:

$$\dot{m}'' = \frac{\dot{Q}''_F + \dot{Q}''_E - \dot{Q}''_L}{L_v} \quad (1)$$

where:

$\dot{m}''$ - burning rate (g/m^2-s)
$\dot{Q}''_F$ - heat flux to the surface from the flame (kW/m^2)
$\dot{Q}''_E$ - external heat flux to the surface (kW/m^2)
$\dot{Q}''_L$ - losses expressed as a heat flux through the surface (kW/m^2)
L_v - heat of gasification (kJ/g)

When burning in air with a constant oxygen concentration, a plot of the measurements of burning rate against external radiation should yield a straight line with a slope of one over the heat of gasification. Figure 5 shows a plot of burning rate against external applied radiant heat flux for the Louisiana crude oil. From this plot the heat of gasification is calculated to be 1.68 kJ/g.

This figure can be used to determine the external radiation that would be necessary to apply in the Cone Calorimeter to generate the same burning rate which was observed in the mesoscale burns. Using the average mesoscale burning rate of 0.047 kg/s/m^2 determined in the next section, an external flux of 71 kW/m^2 applied in the Cone Calorimeter would be required to yield the same burning rate.

7.0 BURNING RATE

The burning of the crude oil was observed to take place in four distinct phases. The four phases were; 1) spreading, 2) steady burning, 3) steady burning with boiling of the water below the oil layer, and (4 transition to extinction. The spreading phase lasted a relatively short period of time as flames spread over the surface from the single ignition point on the upwind side of the pan to cover the entire fuel surface. Once the entire oil surface was covered with flames, the burning continued at a steady rate until the water below the oil surface began to boil. The onset of boiling was characterized by a noticeable increase in sound and bubbles breaking through the oil surface. During boiling the burning rate increased to a steady rate which was greater than the rate prior to boiling. When the fuel was nearly consumed, the fire began a transition to extinction. This was characterized by areas of the oil surface with no visible flames. Frequently, there were oscillations in the burning behavior with increased and decreased burning area and transition to and from boiling. The burning area decreased toward the downwind side of the pan until extinction. A brief chronology of the observed burning behavior for each of the burns is given in table 5.

The average burning rate or the rate at which the oil was consumed during burning was estimated from the burn time and the quantity of oil. For the burns where the manometer operated satisfactorily, the average rate, as well as the rates prior to boiling and during boiling were calculated.

For all burns except the preliminary burn 4/16, the quantity of the oil was determined from the difference in the elevation of the water surface before the oil was added to the pan and the elevation of the oil surface in the pan. For the full pan burns the difference in elevation provided a direct measurement of

the quantity of oil added to the pan. For the partial pan burns, as oil was added to the confined area of the pan the water level in the unconfined area changed since water was free to flow under the timbers or boom used for containment. The hydrostatic head from the water and the oil in the confined area would equal the hydrostatic head from the water in the unconfined area. Equating the hydrostatic heads in the two areas of the pan yields the following expression for the change in the thickness of the oil layer in the confined area of the pan.

$$\Delta h_O = \frac{\Delta h_{O,W}}{1 - \left(\frac{A_T - A_O}{A_T}\right)\Gamma} \tag{2}$$

where:

Δh_O - change in oil layer thickness in the partial pan area (m)

$\Delta h_{O,W}$ - change in the combined oil layer and water thickness in the partial pan area (m)

A_T - total pan area (m^2)

A_o - partial pan area (m^2)

Γ - the ratio of the specific gravity of the oil to the specific gravity of water

For the manometer readings, the measured equivalent water level was converted to oil depth and smoothed using a running 13 point (200 s) running average. The oil surface regression rate was calculated using a least squares linear fit over the time for both the steady burning and steady burning with water boiling phases. The average surface regression rate over the total steady burning phase was determined using a linear fit from the point at which steady burning began to the point at which the transition to extinction began. The specific mass burning rate (rate of mass loss per unit area) was calculated from the surface regression rate and the density of the oil. The heat release rate was determined by multiplying the mass loss rate by the effective heat of combustion for the crude oil (41.9 MJ/kg).

Table 6 gives the initial volume of oil, the volume of residue collected, the volume of oil consumed by burning and the percentage of the initial volume of oil consumed by burning. In the cases where the residue was burned before cleanup the number and duration of the residue burns is shown. The oil consumed includes the total oil consumed during both the primary and residue burns. When burning oil is confined in a towed boom, the oil residue is maintained at a sufficient thickness to support burning. The percent of oil consumed during the mesoscale burns is therefore representative of the percent which would be expected to be consumed if the oil were in a towed boom.

Table 7 shows the average burning rate and surface regression rates based on the measurements of the oil surface level in the pan and the observed burn times. Table 8 gives the same information in customary units. Figure 6 is a plot of the average surface regression rate as a function of the effective burn diameter. From this plot it appears that for the range of diameters used in the mesoscale burns there is no dependency of surface regression rate on burn area. With the exception of the burn with a regression rate of 0.023 mm/s (5/16) and the burn with water spray (5/22) the mean value is 0.055 with a uncertainty of one standard deviation of ± 0.005 mm/s. The rate of 0.023 mm/s is most likely due to measurement error. The mean value for the burning rate per unit area is 0.047 ± 0.004 kg/s/m^2 (4.9 ± 0.4 gal/hr/ft^2) and for the heat release rate per unit area is 1950 ± 175 kW/m^2. The scatter in the regression, burning and heat release rates was due in part to the variable nature of the burns. The wind direction and speed contributed to the wide variation in extinction behavior observed although it did not appear to affect the average

burning rate. In some cases there was a rapid transition from full pan involvement to extinction. In other cases the fire would approach extinction with as little as 5% of the fuel surface covered by flames then return to full involvement. In some cases the wind would corral the remaining fuel in a corner of the pan as the fire approached extinction allowing a significant fraction of the oil to be consumed.

Burn 5/22 which was the burn with water spray showed a slightly higher burning rate than the rest of the burns. When the water spray was initiated it appeared that water reached the surface and the sound was similar to that heard during boiling for the other burns. It is possible that boiling of the water spray on the fuel surface may have enhanced the burning.

The burning rate from the aged oil was nearly same as the average for the fresh oil. This would indicate that short term aging does not effect burning rate.

The burn time used to compute the average burning and surface regression rates was the time from full pan involvement to the beginning of extinction. For burns where an extended period of transition to extinction burning was observed (5/24, 6/4, and 6/5), the effective time of steady burning was adjusted to account for the additional burning during the transition phase. Burn 5/29 exhibited particularly slow initial fire spread and the steady burn time was adjusted to compensate for the oil consumed during that time period.

After completion of all of the burns, the flow meter in the oil transfer line to the pan was found to have been fouled with a piece of foreign matter. The measurements from the flow meter were not used to calculate the burning rate except for burn 4/16. Complete oil surface level measurements were not available for this burn so the volume of fuel was estimated using the flow meter measurements and a correction based on the flow meter measurement for burn 4/17.

Table 9 gives the oil surface regression rate determined from the measurements of the oil surface level and determined from the manometer. In addition, the surface regression rates before and during boiling as determined from the manometer are given. The regression rates determined from the fuel surface measurements are within 6% of the average rates determined from the manometer. The agreement indicates that the methodology used to determine the regression rates from the surface level measurements and the steady burning duration provides good results within the overall accuracy of field experiments. The observation that the regression rates from the surface level measurements are slightly higher than those from the manometer is an indication that a small amount of the fuel was consumed before and after the steady burning period.

Figure 7 shows the average, before boiling and during boiling surface regression rates from the manometer measurements. It can be seen that the burning rate during boiling increased approximately 30% from the burning rate before boiling. This phenomenon has been observed in laboratory experiments and is due to the increased mixing and volatilization of the fuel caused by the boiling of the water under the fuel surface. Also shown in figure 7 are the results from some smaller scale burns which will be discussed in the next section.

The study of crude oil combustion on water is complicated by two factors. One is that the oil is being burned in a layer floating on water. The other is that crude oil is a blend of many hydrocarbons with a wide range of boiling points the majority of which are at greater temperatures than the boiling point of water. Distillation measurements of the Louisiana crude oil show that 90 percent of the compounds in the oil have boiling points above 100 °C. During burning the surface of the crude oil maintains a temperature of around 300 °C. As the fuel is consumed, heat transferred through the fuel to the water below can result in boiling of the water. The boiling effect has been observed in laboratory scale as well

as field scale burns. Boiling of the water below the fuel agitates the fuel layer with both fuel and water droplets being sprayed into the flame, substantially increasing the burning rate of the fire. From previous experiments it appears that boiling resulted in a greater increase in regression rate at the smaller scales[19]. This may be a function of the, oil type, initial oil and water thickness, and other parameters in addition to scale.

8.0 SMOKE YIELD

The quantity of smoke produced from a fire may be expressed as a smoke yield which is defined as the mass of smoke particulate produced from burning a unit mass of fuel. Techniques now exist to measure smoke yield both in the laboratory and in the field.

Three methods were used to determine smoke yield; 1) the flux method, 2) the carbon balance method, and 3) the light extinction method. These methods are discussed in detail by Mulholland, et. al [20], and summarized below. The flux method for determining smoke yield consists of measuring the mass of smoke particulate, m_s, collected on a filter, the mass loss of the fuel burned, m_f, and the ratio of the mass flow of air through the exhaust stack to the mass flow through the filter sample, ϕ. The smoke yield calculated by the flux method is termed ε_1, and is given by the expression

$$\varepsilon_1 = (m_s/m_f)\ \phi \tag{3}$$

The carbon balance method is based on a partial carbon balance, and is the only smoke yield measurement method that can be used both in the laboratory and in the field because it does not require measurement or knowledge of the total combustion product flow. In this method, smoke yield is expressed as the product of the measured fraction of carbon in the fuel, f_c, and the ratio of the measured carbon in the form of smoke particulate to the total carbon mass in the combustion products (CO_2, CO, and smoke aerosols), Y_s. Smoke yield by carbon balance method is denoted by ε_2 and given by

$$\varepsilon_2 = f_c\ Y_s \tag{4}$$

The application of the carbon balance method to smoke yield measurements assumes that in the portion of the combustion product flow from which samples are drawn, both the smoke particulate and gaseous combustion products have been transported together from the combustion zone and their concentrations have been equally diluted by entrained air.

A smoke yield measurement that is completely independent of particulate collection on filters is the light extinction method. This method is based on determining the mass concentration of smoke particulates in a known flow rate of combustion products by measurement of visible light attenuation over a known path length. In this study smoke attenuation measurements were made with a laser photometer. The design of the instrument is described by Babrauskas and Mulholland in reference [21]. The light source used in the instrument is a helium-neon laser with a low flow rate air purge to avoid deposition of soot on the optics. Detector electronics processed the signal and the output was recorded directly in units of extinction coefficient, k (m^1). Calibration was accomplished with known neutral density filters introduced in the beam.

Smoke yield measurements using all three measurement methods in the Cone Calorimeter are presented in table 10. From table 10 it can be seen that there is excellent agreement between all three methods in the Cone Calorimeter. This is most likely because the Cone Calorimeter produces a highly controlled and reproducible fire environment. The largest variation for a single test is ± 6%.

In the field, smoke was drawn by a battery operated pump through a pre-weighed filter which collected the particulates. The clean gas passed through the pump to a set of micrometer adjusted flow control valves which metered and diverted a portion of the gas flow to a 5 liter sample collection bag. A radio controlled switch was used to start and stop the pump remotely as the sampling package was carried into and removed from the fire plume [12]. The filter samples were weighed on a precision balance after the burn and the concentrations of CO_2 and CO in the sample collection bag were determined using a gas chromatograph. In the mesoscale burns, the sampling package was suspended below a tethered miniblimp and was manually maneuvered from the ground and held in the smoke plume downwind of the fire. The altitude and range from the fire are given in table 3. The sample collection times were nominally 600 seconds.

Smoke yields from the mesoscale burns are given in table 11 and smoke yields calculated by the carbon balance method for both scales are shown in figure 8. For the mesoscale burns an estimation of the uncertainty of the smoke yield was determined. The uncertainty interval was based on the accuracy of the balance, the chromatograph and the flow measurements. The uncertainty is shown as error bars in figure 8. From figure 8 it can be seen that smoke yield is dependent on scale. The yield is lower for smaller diameter fires and appears to reach a plateau of approximately 0.13 for fires with diameters above 7 m. In small diameter fires the air which is entrained around the fire perimeter more readily mixes with the fuel resulting in more complete combustion and a lower smoke yield.

The smoke yield from burn 5/17 is distinctly lower than the yields from the other burns. An examination of the start time, sample duration, wind speed and burning rate did not provide an explanation for the low result. The smoke yield for the burn with water spray was less than the yield from four of the burns but greater than the yield from one of the burns. The results are inconclusive and at best the water spray might have reduced the smoke yield slightly, although there was no noticeable difference in smoke production during the burn. Although the smoke yield from the aged oil was on the high side of the values, a definite conclusion concerning the smoke yield from aged oil cannot be reached.

9.0 PARTICLE SIZE DISTRIBUTION

Particulate size is an important health consideration and also impacts the dynamics of smoke settling. Particulates having an aerodynamic effective diameter less than 10 μm are considered respirable [22] and may be drawn into the lungs with normal breathing. In general small particle sizes have the greatest resistance to settling and can be expected to be carried much further from the burn site than larger particles. In addition to the overall particulate yield from the crude oil fires, it is therefore important to have some knowledge about the particulate size distribution. Smoke particles are an agglomeration of individual spherules. The spherules that make up the structure of the smoke particulate are relatively uniform in size with an average diameter of 0.06 μm. Measurements of smoke particles from 3 m diameter crude oil fires have shown a mixture of spherule diameters in two groupings of 0.15 and 0.06 μm [12].

There is no means to directly translate the observed irregular shape of smoke particles into aerodynamic effective diameters. The aerodynamic effective diameter of a particle is defined as the diameter of a smooth spherical particle with a unit density of 1000 kg/m^3 (1 g/cm^3) that has the same settling velocity in air. Therefore, the aerodynamic effective diameter of a particle depends on the size, shape and density of the particle. Cascade impactors measure particle size distribution by the amount of particulate deposited on a series of plates. The particulate laden air is drawn through the cascade impactor which consists of a series of stages each having a nozzle and plate. Aerodynamic forces determine the size ranges that will be deposited on the plate in each stage and the sizes that will pass through to other stages downstream. The fraction of the total deposition collected by each stage of the device determines the distribution of the aerodynamic effective diameter of the particles. The small and light weight commercial impactors used

in this study contained six stages. For cases where a small quantity of particulate is expected, some of the stages may be removed. The cutpoint diameter is the aerodynamic effective diameter that is collected with 50 percent efficiency. Ideally the cutpoint diameter represents the largest diameter particle which will not pass to the next stage but in practice some larger particles do move to the next stage. The cut point diameter is a function of the flow rate through the instrument and decreases with increasing flow rate.

In the mesoscale experiments, the impactor was operated at a flow rate of 0.054 L/s with four stages to assure sufficient particulate deposition in each stage. The cutpoint diameters for each stage were determined using the standard correction methods for the instrument [23]. Table 12 shows the cutpoint diameters for each of the stages in the instrument and the back-up filter at the two flow rates used in this study and figure 9 shown the cumulative size distribution of smoke particulate from a 12.0 m effective diameter fire.

10.0 OIL TEMPERATURE

Temperatures in the oil were measured during some of the burns with a fixed thermocouple array. Figure 10 shows an example of the output from the fixed thermocouple array for burn 5/17. This figure shows the temperatures measured by the thermocouples rising from the initial oil temperature first near the surface and later progressively further into the oil with the temperatures leveling out at approximately 270 °C. As the oil surface dropped below the thermocouples prior to boiling there was a increase in the temperature measured by the thermocouples and then a sharp decrease when boiling began. Figure 11 shows the elevation of the thermocouples relative to the initial oil surface and the time to the initial temperature rise and a temperature of 110 °C as measured by the thermocouples for burn 5/17. For the partial pan burns as the oil is consumed the water level rises and the oil surface regression and water level rise are assumed to be linear during the time from full pan involvement to extinction. Figure 12 shows the same temperature measurements translated to a fixed water level frame of reference. There is a significant uncertainty in the exact location of the thermocouples since the thermocouples had to be positioned before the oil was added to the pan, and the liquid levels were difficult to measure due to waves on the surface and that the water and oil surfaces may not have been level due to the wind. The uncertainty in the position of the thermocouples with respect to the true water and oil surfaces is estimated to be ±10 mm although their position relative to each other is estimated to be within ±1 mm. In figure 12 it can be seem that the initial temperature rise and the increase to 110 °C proceeded through the oil at a rate slightly faster than the surface regression rate. Figures 13, 14, 15 and 16 show the temperature rises measured in burns 5/16 and 5/29 relative to the initial oil surface and translated relative to a fixed water level.

Boiling of the water below the oil was observed in all of the mesoscale burns and in laboratory burns although boiling was not reported in the burn at the Exxon Valdez spill[1]. From observations during laboratory burns in clear containers it appeared that bubbles formed in the water on the underside of the oil and as the boiling became vigorous the bubbles broke through the surface of the oil. The temperatures measured in burns 5/17 and 5/29 confirm earlier laboratory measurements [24] that boiling begins when the water reaches approximately 100 °C. Figure 17 shows the time to boiling as a function of oil depth. With the exception of burn 5/16 which is below and burn 4/17 which is above, the time to boiling is approximately a linear function of initial oil depth with a slope of 0.064 mm/s. As expected, this is greater than the average surface regression rate for the burn series of 0.055 mm/s indicating the thermal penetration is slightly faster than the surface regression. From temperatures measured for burn 5/16 shown in figure 14 the time to boiling would be expected to be approximately 500 seconds which is in agreement with the other burns. The particularly low burning rate for 5/16 indicates that either the initial oil quantity for burn 5/16 was incorrectly measured or there was unaccounted for difference in the burn.

The heat transfer in the burning oil is a complicated process. The oil is a nonuniform mixture of components, is subject to external radiation and is boiling at the surface. Previous efforts to predict the temperature in the oil have not been completely successful [24]. From the measured temperature profiles it can be seen that thermal penetration rate is slow when compared with the surface regression rate. That is indicated by the fact that the initial temperature rise moves at a nearly linear rate through the oil and the rate is only slightly greater than the surface regression rate. This may in part explain the lack observed boiling in the burn at the Exxon Valdez spill. The oil in a towed boom is continually corralled at the back of the boom and as the oil is consumed, the burn area decreases rather than just the oil thickness as in the mesoscale burns. This maintains at least the minimum oil thickness to sustain burning but decreases the likelihood that sufficient heat can be transferred through the oil to the water to initiate boiling. Further, as the oil is moving with respect to the water, cool water is continuously being introduced beneath the oil.

11.0 WATER TEMPERATURE

Figure 18 shows the average water temperature profile for the 60 seconds prior to the beginning of extinction for burn 5/31. The error bars represent the fluctuation in the temperature measurements over the 60 second period. Since this was a full pan burn no correction for the water level was required. From this figure it can been seen that there is little or no temperature increase in the water more than approximately 30 mm below the surface. The heat transfer in the water is a complex process due to boiling, radiation and turbulence. The simplest approximation of the heat transfer is to assume one-dimensional conduction with the water acting as a semi-infinite solid and a step change in surface temperature. The governing equation is:

$$\frac{\partial^2 t}{\partial x^2} = \frac{1}{\alpha}\frac{\partial t}{\partial \theta} \tag{5}$$

with initial and boundary conditions of:

$$t(0,\theta) = t_c$$

$$\lim_{x \to \infty} = t_i$$

$$t(x,0) = t_i$$

where:

t - temperature

t_c - the temperature of the water/oil interface

t_i - initial temperature of the water

x - distance

θ - time

α - thermal diffusivity

The solution is [25]:

$$t(x,\theta) = t_i + (t_c - t_i)\ erfc\frac{x}{2\sqrt{\alpha\theta}} \qquad (6)$$

where:
erfc - complementary error function.

The prediction with this solution is plotted in figure 18 using a thermal diffusivity of water of 1.59×10^{-7} m^2/s, an initial water temperature of the water of 30 °C, and a water surface temperature of 100 °C. The predicted temperature was aligned to agree with the thermocouple which most closely measured 100 °C and therefore was most likely actually at the water surface. Although the use of the one-dimensional semi-infinite solution neglects many of the complexities expected in the heat transfer, it provides a remarkably good approximation of the temperature profile in the water after boiling begins.

Temperatures were measured in the water before and after some of the burns with a portable thermocouple array and in both the oil and water during some of the burns with the fixed thermocouple array. Tables 16 and 17 give the water temperatures measured with the portable thermocouple array. The tables give the time before ignition or after extinction at which the measurements were made and the location of the measurements. All measurements were made approximately 600 mm from the wall of the pan. Due to the presence of oil residue, the measurements could not always be made in the same location. For the partial pan burns one of the measurements was made in the burn area and one in corner farthest from the burn area.

The thermocouple array was placed on the bottom of the pan and the elevation of the measurement points is with respect to the bottom of the pan. A temperature measurement was made at the water surface and the approximate elevation of the water surface is indicated in parenthesis. The variation in the elevation of the water is primarily due to the uneven bottom of the pan and to a lesser extent the movement of the pan during the burn and wind induced movement of the water. As a result, although the vertical measurement locations reflect the local elevation within ±2 mm, the difference between the elevation measured and the elevation of a level plane is estimated to be within ±10 mm.

The water temperature measurements with the portable thermocouple array show that the water temperature in the pan before ignition was uniform with depth and uniform across the pan. The water temperature in the burn area after the fire generally increased 20-30 °C at the surface, 5-10 °C, 35-50 mm below the surface, 1-4 °C, 115-130 mm below the surface, and increased 1 °C or less at distances greater than 190 mm below the surface. For the partial pan burns the water temperature outside the burn area generally increased less than 8 °C at the surface, less than 7 °C, 35-50 mm below the surface, and increased 1 °C or less at distances greater than 115 mm below the surface. In most cases the water temperatures after the fire reflect the influence of the wind direction on the flames with the temperatures being hotter on the downwind side.

The temperature measurements with the portable thermocouple array show the increase in water temperature to be limited to the area very close to the fire and with substantial temperature increase limited to within 35-50 mm of the water surface for burns with a total duration of up to 2465 seconds in a confined pan. These are in agreement with the profile directly under the oil measured for in burn 5/31. For burns in open water it could be expected that water motion and the movement of the burning oil on the water surface would result in somewhat lower increases in water temperatures.

12.0 FIRE PULSATIONS

A natural phenomenon associated with all buoyant diffusion flames is the regular pulsation of the flame caused by interactions with air flow near the base of the flame. For small fires this "flicker" of the flame is well known. Larger laboratory fires also have regular pulsations that generate large scale structures in the smoke plume flow. The frequency of these pulsations (vortex shedding frequency) has been correlated for fire diameters from 0.03 m to 50 m by the equation [26]:

$$f = \frac{1.5}{\sqrt{D}} \tag{7}$$

where:
f - pulsation frequency (Hz)
D - effective diameter of the fire (m)

This correlation shows there is a strong decrease in the frequency of the pulsations with increasing diameter of the fire. In measurements using a gas burner, Hamins [27] has shown that the pulsation frequency of flames was not sensitive to a factor of two variation in heat release rate with a constant exit velocity of the fuel, although wind is thought to lead to substantial changes in the pulsation frequency [28].

Video recordings of the mesoscale experiments were analyzed to determine the pulsation frequency of the fire by observing the motion of the flame near the fuel surface. Table 13 lists the measured values of pulsation frequency with the range of the measurements, the predicted frequency, the effective fire diameter and the near surface wind speed. For some of the burns, a pulsation frequency before and after the onset of boiling was measured. In two of the three experiments in which the burning continued for sufficient time after the onset of boiling to measure the pulsation frequency, no significant increase was found. For the smallest burns (effective diameter of 6.88 m) an increase of almost a factor of three in wind speed did not significantly change the pulsation frequency of the fire. Measurements are generally in agreement with predictions using equation (7) and the data from other fires given in reference [26]. The largest variation, about 1/3 of the predicted frequency, occurred for the 17.2 m effective diameter burn.

13.0 SMOKE PLUME TRAJECTORY MEASUREMENTS

Although there are many accidental fires that produce smoke plumes, these opportunities are not useful for gathering data that is needed to validate predictive methods for smoke plume trajectory and particulate deposition. This is because the smoke production and heat release rates of the fire are unknown. The mesoscale pan fire burns provided a unique opportunity to measure smoke plume trajectories for burns of known particulate emission and fuel burning rates. Measurements of smoke plume trajectories were made in half of the mesoscale burns. The trajectory and radius of the smoke plume were measured using video recordings and subsequently analyzed using digital image processing. Results of these measurements and discussion of the data reduction techniques have been reported by Leonard, et al. [29].

Ideally, measurement of smoke plume trajectory and cross section would be performed using a combination of near field ground observations and long-range measurement from an aircraft following the plume downwind. Near-field ground based measurements were used in this study to measure the initial plume trajectory and cross section over a distance of 1 to 2 km from the source. Both video and still photography images of the initial rise of the smoke plume from the pan were recorded. Distances on these images were scaled from known distances between fixed objects in the field of view.

Since it was not always practical to view the smoke plume perpendicular to the direction of flow, adjustments for oblique viewing angles were made during the data analysis. Figure 19 shows the geometric correction to the observed plume length from a camera at an oblique angle to the wind-blown plume direction. The true plume length (a') is calculated from the observed length (a) as:

$$a' = a/\sin\beta \tag{8}$$

where β is the angle between the nominally crosswind camera view and the smoke plume centerline direction.

The plume radius as a function of distance from the source was measured from photographic images taken upwind of the fire. At selected segments of the plume (see figure 20), the radius of the plume was determined at seven locations equidistant along the plume centerline. The highest and lowest values were ignored, and the remaining five values were averaged as the best estimate for the radius of that segment. Each segment can be approximated as a cylinder with radius equal to the average radius of the segment, and length equal to the length of the segment. The volumes of the segments can be added together over the entire length of the plume to estimate the total plume volume as:

$$V_p = \sum_{n=1}^{N} \pi r_n^2 l_n \tag{9}$$

where:

V_p - volume of the plume
n - segment number
N - total number of segments
r - radius of a cylindrical segment
l - length of a cylindrical segment

Of the experiments in which measurements were made, mesoscale burn 5/30 provided data on plume trajectory for the largest distance from the pan. As listed in table 4, for this burn the wind direction was from the south-south-east at 170 degrees from magnetic north. The nominal wind speed was 3 m/s at 2 m above ground and 6.2 m/s at 48 m above ground. The crosswind camera recording the plume images was located 3500 m from the pan to the north-east, 70 degrees from magnetic north (across Mobile Bay). Therefore, the crosswind camera was nearly perpendicular to the plume direction. The angle (β) between the camera viewing direction and the plume was 80 degrees. Figure 21 shows a sequence of plume photographs taken from the crosswind camera and the corresponding digitized images at one minute intervals for the first five minutes after ignition. This shows good agreement between the visual plume and the images used for digital analysis. Figure 22 shows digitized images of the plume used for volume and trajectory analysis over the first 600 s after ignition.

Table 14 summarizes the results for plume rise, plume volume, and rate increase in plume volume. Measured plume rise heights for the first 600 s after ignition are plotted in figure 23. At 600 s after ignition the leading edge of the smoke plume had risen to 780 m and traveled 1800 m downwind from the pan. The estimated total volume of the plume at 600 s after ignition was 3.8×10^8 m^3. At that time, the total volume of the smoke plume was increasing at a rate of 3.2×10^6 m^3/s. This rate of volume increase is largely the result of mixing of smoke particulate in the plume with surrounding air as opposed to the injection of newly formed smoke particulate from the burning crude oil. Table 15 lists the radii of the plume for various downwind distances as determined from analysis of the digitized image of the plume 10 minutes after ignition. These data show the expansion of the smoke plume depth from 40 m near the source to 820 m near the leading edge, 1820 m downwind from the source.

14.0 SUMMARY AND CONCLUSIONS

For the mesoscale experiments, the average burning rate for fresh Louisiana crude oils at 17.2 m effective diameter was only 7% greater than that measured at the largest laboratory scale of 2.0 m. This indicates that with small corrections the burning rates of large laboratory fires can be used to estimate the expected steady burning of larger fires. The wind speed did not appear to affect the average burning rate but did contribute to variations in burning extinction. The recommended value to use for the burning rate of thick layers of fresh crude oils on water is 0.047 ± 0.004 kg/s/m^2 (4.9 ± 0.4 gal/hr/ft^2).

It was generally found that well over 90 percent of the fresh oil was consumed in the pan burns. In addition, the residue from the primary burn could be corralled and burned with the addition of kerosene as an ignitor.

Smoke yield from fresh crude oil fires depends on diameter. In 0.085 m diameter laboratory fires the minimum smoke yield of 0.06 (kg smoke particulate/kg fuel burned) for Louisiana crude oil was measured. Measurement from the mesoscale experiments are more scattered than the 0.85 m diameter measurements, but the value of 0.13 ± 0.01 smoke yield represents most of the mesoscale measurements.

The size distributions of aerodynamic effective diameters for the smoke particulate were measured in the mesoscale fires. Ninety percent of the particulate mass was below 10 μm in diameter as measured with a cascade impactor.

The measured oil temperature profiles show that thermal penetration rate is slow when compared with the surface regression rate. That is indicated by the fact that the initial temperature rise moves at a nearly linear rate through the oil and the rate is only slightly greater than the surface regression rate. Boiling was observed when water beneath the oil reaches approximately 100 °C. The use of the one-dimensional semi-infinite heat transfer solution provides a remarkably good approximation of the temperature profile in the water beneath the oil after boiling begins even though it neglects many of the complexities expected in the heat transfer.

Ground level photographic images of the plume taken nearly perpendicular to the wind direction and upwind of the fire were digitized and used to estimate the plume rise and volume. For this technique to be successful the images must include reference points with known separation distances and a reference point with a known elevation so that angle corrections can be calculated.

15.0 ACKNOWLEDGEMENTS

This work was a continuation of studies begun in 1985 as part of the Technology Assessment and Research Program for Offshore Minerals Operations managed by John Gregory and Ed Tennyson of Minerals Management Service. The research was funded jointly by the Minerals Management Service, U.S. Department of the Interior, the American Petroleum Institute, and the U.S. Coast Guard, Department of Transportation. Special technical assistance and cooperation was provided by Merv Fingas of the Technology Development and Technical Services Branch, Environment Canada and the Rod Terpin of the Environmental Protection Agency, Emergency Response Team in Edison, NJ. David D. Evans of NIST was the project manager.

The cooperation and hospitality of the U.S. Coast Guard Research and Development Center and the Fire and Safety Test Detachment in preparing for and conducting the mesoscale burning experiments has been outstanding in every respect.

Donations of crude oil for the mesoscale experiments were made by Exxon Baton Rouge Refinery and BP America. Special measurement, testing, and analysis equipment in addition to profession staff time were provided to this project by EPA-ERT, ACS, 3M, NOAA, LSU.

Dr. James Morehart formerly of the Building and Fire Research Laboratory, NIST provided essential assistance in the design of measurement methods and analysis of the data from the mesoscale experiments. Richard Peacock contributed substantially to the analysis of burning rate data from the mesoscale burns. J. Randall Lawson provided the smoke yield calculations.

David D. Evans, J. Randall Lawson, Kathy Notarianni, William Twilley, Jay McElroy, and Roy McLane of the Building and Fire Research Laboratory, NIST provided immeasurable assistance in conducting the mesoscale burns.

Edward Budnick and Jerry Back of Hughes Associates provided detailed measurements and analysis of the smoke plume trajectories and shapes that were needed as part of the evaluation of the two predictive models for smoke dispersion.

The program of mesoscale burn experiments was coordinated through the Burn Evaluation Steering Team (BEST).

16.0 REFERENCES

1. Allen, A.A., "Contained Controlled Burning of Spilled Oil During the Exxon Valdez Spill," Proceedings of the Thirteenth Arctic and Marine Oil Spill Program Technical Seminar, June 6-8, 1990, Edmonton, Alberta, Ministry of Supply and Services Canada, Cat. No. En 40-11/5-1990. pp. 305-313, 1990.

2. Robertson, I., "Operational Examples of In-Situ Burning: Lessons from the Burning of Two Recent Diesel Spills on the B.C. Coast," Proceedings of the Fourteenth Arctic and Marine Oil Spill Program Technical Seminar, June 12-14, 1991, Vancouver, British Columbia, Ministry of Supply and Services Canada, Cat. No. EN 40-11/5-1991, pp. 411-419, 1991.

3. Thompson, C.H., Dawson, G.W., and Goodier J.L., "Combustion: An Oil Spill Mitigation Tool," U.S. Dept. of Energy, Contract No. EY-76-C-06-1830, 1979

4. Brown, H.M. and Goodman, R.H., "In Situ Burning of Oil in Ice Leads," Proceedings of the Ninth Annual Arctic and Marine Oilspill Program Technical Seminar, June 10-12, 1986, Edmonton, Alberta, Canada, Environment Canada, Ottawa K1A 0H3, 1986.

5. Smith, K.N. and Diaz, A., "In-Place Burning of Crude oil in Broken Ice: 1985 Testing at OHMSETT," Proceedings of the Eight Annual Arctic Marine Oilspill Program Technical Seminar, June 18-20, 1985, Edmonton, Alberta, Canada, Environment Canada, Ottawa K1A 0H3, 1985.

6. Buist, I.A. and Twardus, E.M., "Burning Unconfined Oil Slicks: Large Scale Tests and Modelling," Proceedings of the Eight Annual Arctic Marine Oilspill Program Technical Seminar, June 18-20, 1985, Edmonton, Alberta, Canada, Environment Canada, Ottawa K1A 0H3, 1985.

7. Evans, D., Baum, H., McCaffrey, B., Mulholland, G., Harkleroad, M., and Manders, W., "Combustion of Oil on Water," Proceedings of the Ninth Arctic Marine Oilspill Program

Technical Seminar, June 10-12, 1986, Edmonton, Alberta, Ministry of Supply and Services Canada Cat. No. En 40-11/5-1986E, pp. 301-336, 1986.

8. Evans, D., Mulholland, G., Gross, D., Baum, H., and Saito, K., "Environmental Effects of Oil Spill Combustion," Proceedings of the Tenth Arctic and Marine Oilspill Program Technical Seminar, June 9-11, 1987, Edmonton, Alberta, Ministry of Supply and Services Canada Cat. No. En 40-11/5-1987E, pp. 91-130, 1987.

9. Evans, D., Mulholland, G., Gross, D., Baum, H., and Saito, K., "Burning, Smoke Production, and Smoke Dispersion from Oil Spill Combustion," Proceedings of the Eleventh Arctic and Marine Oil Spill Program Technical Seminar, June 7-9, 1988, Vancouver, British Columbia, Ministry of Supply and Services Canada, Cat. No. En 49-11/5-1988 E/F, pp. 41-87, 1988.

10. Evans, D., Baum, H., Mulholland, G., Bryner, N., and Forney, G., "Smoke Plumes From Crude Oil Burns," Proceedings of the Twelfth Arctic and Marine Oil Spill Program Technical Seminar, June 7-9, 1989, Calgary, Alberta, Ministry of Supply and Services Canada, Cat. No. En 40-11/5-1989, pp. 1-22, 1989.

11. Evans, D., Walton, W., Baum, H., Lawson, R., Rehm, R., Harris, R., Ghoniem, A., Holland, J., "Measurement of Large Scale Oil Spill Burns," Proceedings of the Thirteenth Arctic and Marine Oil Spill Program Technical Seminar, June 6-8, 1990, Edmonton, Alberta, Ministry of Supply and Services Canada, Cat. No. En 40-11/5-1990. pp. 1-38, 1990.

12. Evans, D., Walton, W., Baum, H., Mulholland, G., Lawson, J., Koseki, H., and Ghoniem, A., "Smoke Emission from Burning Crude Oil," Proceedings of the Fourteenth Arctic and Marine Oil Spill Program Technical Seminar, June 12-14, 1991, Vancouver, British Columbia, Ministry of Supply and Services Canada, Cat. No. EN 40-11/5-1991, pp. 421-449, 1991.

13. Evans, D., Tennyson, E.J., In-Situ Burning -- A Promising Oil Spill Response Strategy, Seventh Symposium on Coastal and Ocean Management, July 8-12, 1991, Long Beach, California, conference preprint, 1991.

14. Evans, D., Walton, W., Baum, H., Notarianni, K., Lawson, J., Tang, H., Keydel, K., Rehm, R., Madrzykowski, D., Zile, R., Koseki, H., and Tennyson E., "In-Situ Burning of Oil Spills: Mesoscale Experiments," Proceedings of the Fifteenth Arctic and Marine Oil Spill Program Technical Seminar, June 10-12, 1992, Edmonton, Alberta, Ministry of Supply and Services Canada, Cat. No. En 40-11/5-1992. pp. 593-657, 1992.

15. Li, K., Caron, T., Landriault, M., Paré, J.R.J., and Fingas, M., "Measurement of Volatiles, Semi-volatiles and Heavy Metals in an Oil Burn Test," Proceedings of the Fifteenth Arctic and Marine Oil Spill Program Technical Seminar, June 10-12, 1992, Edmonton, Alberta, Ministry of Supply and Services Canada, Cat. No. En 40-11/5-1992. pp. 561-573, 1992.

16. Jones, R.K., Farr, J., Simecek-Beatty, D., Carney, K., Roques, D., Henry, C., and Overton, E., The Evaporation of Benzene and a Series of Alkanes from Crude Oil, Hazard Materials and Response Division, NOAA, Seattle, WA, HMARD Report 92-5, 1992.

17. Babrauskas, V., The Cone Calorimeter -- A New Tool for Fire Safety Engineering, ASTM Standardization News, Vol 18, pp. 32-35, 1990.

18. Drysdale, D., An Introduction to Fire Dynamics, John Wiley and Sons, Chichester, England, 424 p., 1985.

19. Benner, B. A. Jr., Bryner, N. P., Wise, S. A., Mulholland, G. W., Lao, R. C., Fingas, M. F., "Polycyclic Aromatic Hydrocarbon Emissions from the Combustion of Crude Oil on Water," Environmental Sciences & Technology, Vol. 24, pp. 1418-1427, 1990.

20. Mulholland, G.W., Henzel, V., Babrauskas, V., The Effect of Scale on Smoke Emissions, Fire Safety Science -- Proceedings of the Second International Symposium, Hemisphere Publishing Corporation, New York, pp.347-357, 1989.

21. Babrauskas, V., Mulholland, G., Smoke and Soot Data Determinations in the Cone Calorimeter, Mathematical Modeling of Fires, ASTM STP 983, American Society for Testing and Materials, Philadelphia, pp. 83-104, 1987.

22. Hering, S.V. (editor), Air Sampling Instruments for Evaluation of Atmospheric Contaminates, 7th Edition, American Conference of Governmental Industrial Hygienists, Cincinnati, Ohio, 612 p., 1989.

23. Marple Personnel Cascade Impactors, Series 290, Instrument Manual, Bulletin No. 290I.M.-3-82, Sierra Instruments, Inc, Carmel Valley, CA.

24. Inamura, T., Satio, K., and Tagavi, K.A., A Study of Boilover in Liquid Pool Fires Supported on Water. Part II: Effects of In-depth Radiation Absorption, Comb. Sci. Tech. 86, 105-119, 1992.

25. Myers, G.E., Analytical Methods in Conduction Heat Transfer, McGraw Hill, New York, NY, 508 p., 1971.

26. Pagni, P.J., Fire Modeling, Grant Report, Summaries of BFRL Fire Research Program In-House Projects and Grants, 1991, Nora Jason, Editor, National Institute of Standards and Technology, Gaithersburg, MD, pp.57-60, 1991.

27. Hamins, A., Yang, J.C., Kashiwagi, T., An Experimental Investigation of the pulsation Frequency of Flames, 24th Symposium (International) on Combustion, The Combustion Institute, Pittsburgh, PA., to appear.

28. Gengembre, E., Cambray, P., Karmed, D., Bellet, J.C., Turbulent Diffusion Flames with Large Buoyancy Effects, Comb. Sci. Tech. 41, 55, 1984.

29. Leonard, J.T., Budnick, E.K., Back, G.G., Garney, S.J., Development of a Video Image-based Methodology for Estimating Large Scale Hydrocarbon Smoke Plume Size and Extent, Naval Research Laboratory, in preparation.

Table 1. Louisiana crude oil properties

Property	**Value (measured by independent laboratories)**
Specific Gravity	sample 1 - 0.8453 sample 2 - 0.8448
API Gravity @ 15.6 °C (60 °F)	sample 1 - 35.9 sample 2 - 36.0
Kinematic Viscosity @ 37.8 °C (100 °F)	5.49 mm^2/s (5.49 cSt)
Reid Vapor Pressure	26.9 kPa (3.9 lbf/in^2) absolute
Flash Point - Pensky Martin Closed Cup	less than ambient
Carbon mass fraction	0.862 ± 0.2%
Hydrogen mass fraction	0.134 ± 1.6%
Sulfur mass fraction	0.000

Table 2. Mesoscale burn size

Burn No.	Burn Size (m)	Burn Area		Effective Burn Diameter		Burn Area/ Full Pan Area (%)	Features
		(m^2)	(ft^2)	(m)	(ft)		
4/16	6.10 × 6.10	37.2	400	6.88	22.6	16	
4/17	6.10 × 6.10	37.2	400	6.88	22.6	16	
5/16	6.10 × 6.10	37.2	400	6.88	22.6	16	
5/17	6.10 × 6.10	37.2	400	6.88	22.6	16	
5/22	10.7 × 10.7	114	1225	12.0	39.4	49	water spray
5/23	11.9 × 15.2	181	1950	15.2	49.9	78	boom attached two ends, free to move
5/24	11.2 × 15.2	170	1830	14.7	48.2	74	boom attached two ends, free to move
5/28	8.53 × 8.53	72.8	784	9.63	31.6	32	boom attached two ends, restricted to square area
5/29	6.10 × 6.10	37.2	400	6.88	22.6	16	oil aging
5/30	10.7 × 10.7	114	1225	12.0	39.4	49	
5/31	15.2 × 15.2	231	2490	17.2	56.4	100	
6/3	10.7 × 10.7	114	1225	12.0	39.4	49	
6/4	10.7 × 10.7	114	1225	12.0	39.4	49	
6/5	15.2 × 15.2	231	2490	17.2	56.4	100	

Table 3. Mesoscale airborne samples

Burn No.	Miniblimp No.	Samples	Start Time (s)	Total Time (s)	Range (m)	Altitude (m)
4/16	1.1	PAH, TEM grid	29	425	61	128
	1.2	smoke yield	1165	245	61	128
4/17	1.1	Formaldehyde, charcoal tube	17	529	61	56
	1.2	PAH, TEM grid	641	226	61	56
5/16	1	PAH	48	1273	56	44
5/17	1	smoke yield	215	681	106	100
5/22	1	smoke yield	107	403	83	38
5/23	1	PAH	--:--	617	48	30
5/28	1.1	quartz filter #1	-10	248	87	45
	1.2	quartz filter #2	436	163	87	45
5/29	1	smoke yield	155	692	47	16
5/30	1	impactor, TEM grid	0	1152	87	45
	2.1	quartz filter	28	210	87	45
5/31	2.1	quartz filter	20	429	103	150+
6/3	1	PAH, charcoal tube	32	1515	109	150+
	2	smoke yield	71	722	109	150+
6/4	1.2	PAH, impactor	387	948	109	160
	2	formaldehyde, charcoal tube, passive filter	12	1351	109	160
6/5	1.1	smoke yield, TEM grid	59	915	100	121
	1.2	PAH, charcoal, passive filter	1134	868	100	121
	2	PAH, passive filter	109	1883	100	121

Note: All times from ignition

Table 4. Mesoscale meteorological conditions

Burn No.	Ground Weather Station					Airborne Weather Station			
	Wind Speed. (m/s)	Wind Dir. (°)	Temp. (°C)	R.H. (%)	B.P. (kPa)	Alt. (m)	Wind Speed (m/s)	Wind Dir. (°)	Temp. (°C)
4/16	1.5	117	25.3	74	101.9	NA	NA	NA	NA
4/17	1.9	150	24.0	73	101.6	NA	NA	NA	NA
5/16	2.1	141	27.0	81	101.4	50	5.3	150	25.2
5/17	1.7	165	26.3	69	101.5	50	3.9	141	25.2
5/22	4.0	57	24.3	87	101.3	NA	NA	NA	NA
5/23	5.0	107	25.3	85	NA	NA	NA	NA	NA
5/24	2.4	134	25.9	89	NA	51	6.0	120	24.3
5/28	1.2	206	27.5	92	101.8	48	4.1	189	25.3
5/29	5.0	189	30.1	72	101.6	41	9.8	196	26.0
5/30	3.9	168	28.7	72	101.5	48	6.2	168	25.6
5/31	0.8	40	27.3	81	101.4	52	1.3	49	24.5
6/3	1.0	61	26.4	74	NA	NA	NA	NA	NA
6/4	2.1	177	30.2	72	NA	NA	NA	NA	NA
6/5	2.1	41	30.3	69	NA	NA	NA	NA	NA

NA - not available

Table 5. Mesoscale burn chronology

Burn No.	Effective Burn Diameter (m)	Initial Oil Depth (mm)	Time to Full Involvement (s)	Time to Begin Boiling (s)	Time to Begin Extinction (s)	Time to Extinction (s)
4/16	6.88	90	40	663	1588	1673
4/17	6.88	43	20	564	671	812
5/16	6.88	34	30	1008	1186	1270
5/17	6.88	60	13	850	1135	1267
5/22	12.0	32	62	NA	466	855
5/23	15.2	18	104	220	423	700
5/24	14.7	33	85	270	630	1203
5/28	9.63	31	38	387	486	613
5/29	6.88	62	241	761	1186	1455
5/30	12.0	51	42	591	1035	1082
5/31	17.2	49	15	596	950	1068
6/3	12.0	63	27	825	1215	1251
6/4	12.0	61	47	654	769	1200
6/5	17.2	62	32	641	855	2465

Note: All times from ignition

Table 6. Mesoscale oil volume

Burn No.	Crude		Residue		Consumed		Consumed (%)	Residue burns
	(m^3)	(gal)	(m^3)	(gal)	(m^3)	(gal)		
4/16	3.36[1]	887	0.23	60	3.13	827	93	
4/17	1.60	423	0.10	25	1.50	398	94	
5/16	1.30	343	0.33	88	0.97	255	75	
5/17	2.25	594	0.17	44	2.08	550	92	
5/22	3.37	969	0.12	32	3.25	937	96	
5/23	3.31	875	0.33	88	2.98	787	90	
5/24	5.56	1470	0.12	30	5.44	1440	98	
5/28	2.25	594	0.16	41	2.09	553	93	
5/29	2.31	610	0.21	55	2.1	555	91	
5/30	5.80	1530	0.07	18	5.73	1510	99	1st - 1318 s 2nd - not recorded
5/31	11.8	3110	0.16	43	11.6	3065	99	1st - 1054 s 2nd - 460 s
6/3	7.22	1910	0.10	26	7.12	1880	99	1st - 769 s 2nd - 304 s 3rd - 401 s
6/4	6.98	1845	0.30	81	6.68	1765	96	
6/5	14.1	3720	0.14	37	14.0	3680	99	456 s

[1] Estimated from flow meter

Note: Residue quantities after residue burns if applicable

Table 7. Mesoscale average burning rate

Burn No.	Effective Burn Diameter (m)	Burn Time (s)	Oil Consumed		Average Burning Rate			Average Surface Regression Rate
			(kg)	(m^3)	($kg/s/m^2$)	(kW/m^2)	MW	(mm/s)
4/16	6.88	1548	2645[1]	3.13	0.046	1925	72	0.054
4/17	6.88	651	1270	1.50	0.052	2195	82	0.062
5/16	6.88	1156	820	0.97	0.019	799	30	0.023
5/17	6.88	1122	1760	2.08	0.042	1765	66	0.050
5/22	12.0	404	2745	3.25	0.060	2500	285	0.071
5/23	15.2	319	2520	2.98	0.044	1825	331	0.052
5/24	14.7	645[2]	4600	5.44	0.042	1755	299	0.049
5/28	9.63	448	1765	2.09	0.054	2270	165	0.064
5/29	6.88	1045[3]	1775	2.10	0.046	1910	71	0.054
5/30	12.0	993	4840[4]	5.73	0.043	1790	204	0.051
5/31	17.2	935	9800[4]	11.6	0.045	1900	439	0.054
6/3	12.0	1188	6015[4]	7.12	0.044	1860	212	0.053
6/4	12.0	1020[2]	5645	6.68	0.049	2030	232	0.057
6/5	17.2	1000[2]	11830[4]	14.0	0.051	2145	496	0.061

[1] Estimated from flow meter
[2] Effective burn time due to long-term intermittent burning at end of the burn
[3] Effective burn time due to slow initial fire spread
[4] Residue was burned

Table 8. Mesoscale average burning rate (customary units)

Burn No.	Effective Burn Diameter (ft)	Burn Time (s)	Oil Consumed (gal)	Initial Oil Thickness (in)	Average Burning Rate (gal/hr/ft^2)	Average Surface Regression Rate (in/min)
4/16	22.6	1548	827[1]	3.5	4.8	0.13
4/17	22.6	651	398	1.7	5.4	0.15
5/16	22.6	1156	255	1.4	2.0	0.05
5/17	22.6	1122	550	2.4	4.4	0.12
5/22	39.4	404	937	1.3	6.3	0.17
5/23	49.9	319	787	0.7	4.6	0.12
5/24	48.2	645[2]	1440	1.3	4.4	0.12
5/28	31.6	448	553	1.2	5.6	0.15
5/29	22.6	1045[3]	555	2.4	4.8	0.13
5/30	39.4	993	1510[4]	2.0	4.5	0.12
5/31	56.4	935	3065[4]	1.9	4.7	0.13
6/3	39.4	1188	1885[4]	2.5	4.6	0.13
6/4	39.4	1020[2]	1765[4]	2.4	5.1	0.13
6/5	56.4	1000[2]	3680[4]	2.4	5.3	0.14

[1] Estimated from flow meter
[2] Effective burn time due to long-term intermittent burning at end of the burn
[3] Effective burn time due to slow initial fire spread
[4] Residue was burned

Table 9. Mesoscale average oil surface regression rate

Burn No.	Effective Burn Diameter (m)	Burn Time (s)	Oil Consumed (kg)	Surface Regression Rate			
				From Manometer			From Fuel Level
				Before Boiling (mm/s)	During Boiling (mm/s)	Average (mm/s)	Average (mm/s)
5/31	17.2	935	9800[2]	0.045	0.060	0.051	0.054
6/3	12.0	1188	6015[2]	0.049	0.061	0.053	0.053
6/5	17.2	1000[1]	11830[2]	0.054	0.073	0.059	0.061

[1] Effective burn time due to long-term intermittent burning at end of the burn
[2] Residue was burned

Table 10. Smoke yield measured in the Cone Calorimeter

Cone Test No.	Flux Method ε_1	Carbon Balance Method ε_2	Light Extinction Method ε_3	Test Average
1	0.063	0.067	0.060	0.063 ± 6%
2	0.058	0.062	0.061	0.060 ± 3%
3	0.063	0.068	0.062	0.064 ± 6%

Table 11. Smoke yield from mesoscale burns

Burn No.	Effective Diameter (m)	Smoke Yield	Uncertainty Interval
4/6/91	6.88	0.137	0.123 - 0.152
5/17/91	6.88	0.079	0.070 - 0.085
5/22/91 Water spray	12.0	0.103	0.090 - 0.119
5/29/91 Aged Oil	6.88	0.137	0.128 - 0.146
6/3/91	12.0	0.121	0.109 - 0.135
6/5/91	17.2	0.127	0.109 - 0.154

Table 12. Cascade impactor stage cutpoint size diameters

Flow Rate (L/s)	Stage 1 µm	Stage 2 µm	Stage 3 µm	Stage 4 µm	Stage 5 µm	Stage 6 µm	Back-up Filter µm
0.054	7.8	---	---	1.2	0.70	0.39	0

Table 13. Pulsation frequency of pool fires

Burn	Effective Diameter (m)	Wind Speed (m/s)	Frequency Before Boiling (Hz)	Frequency During Boiling (Hz)	Predicted Frequency Eqn. (7) (Hz)
5/17	6.88	1.7	0.73±0.08	---	0.57
5/29	6.88	5.0	0.70±0.04	---	0.57
6/3	12.0	1.0	0.42±0.03	0.56±0.07	0.43
6/4	12.0	2.1	0.42±0.07	0.45±0.05	0.43
5/31	17.2	0.8	0.46±0.04	0.44±0.04	0.36

Table 14. Initial smoke plume characteristics for mesoscale burn 5/30

Elapse Time (s)	Height (m)	Distance (m)	Volume ($m^3 \times 10^6$)	Volume Rate of Change ($m^3/s \times 10^6$)
120	160	430	1.8	0.015
240	380	730	10.4	0.072
360	480	1130	58	0.39
480	660	1350	130	1.1
600	780	1820	380	3.2

Table 15. Height and radii of the smoke plume 10 minutes after ignition for burn 5/30

Downwind Distance (m)	Centerline Height (m)	Effective Diameter (m)
0	0	0
110	40	40
210	80	130
320	120	230
430	160	320
540	200	420
640	240	400
750	310	610
860	380	540
970	440	460
1070	510	480
1180	580	550
1290	640	640
1390	670	730
1500	700	820
1610	730	780
1720	750	720
1820	780	820

Table 16. Water temperatures, burns 5/24, 5/28, and 5/30

	Burn Number 5/24 14.7 m effective diameter				Burn Number 5/28 9.63 m effective diameter				Burn Number 5/30 12.0 m effective diameter			
	Time before ignition (s)		Time after extinction (s)		Time before ignition (s)		Time after extinction (s)		Time before ignition (s)		Time after extinction (s)	
	3130	3220	1230	NA	3140	2910	770	1140	3460	3100	510	740
	Position				Position				Position			
	West side south of burn area	SE corner of pan	West side south of burn area	SE corner of pan	SW corner of burn area	SE corner of pan	Center of west side of pan	SE corner of pan	Center of west side of pan	SE corner of pan	SW corner of burn area	SE corner of pan
Elevation (mm)	Water temperature (°C)				Water temperature (°C)				Water temperature (°C)			
surface (elevation mm)	27.3 (510)	26.3 (485)	46.7 (510)	34.3 (510)	26.7 (510)	26.4 (460)	43.9 (495)	26.7 (470)	29.1 (485)	29.3 (485)	59.8 (495)	30.1 (485)
460	26.8	26.7	38.0	34.0	26.1	26.4	28.9	27.0	29.5	29.4	35.6	30.4
380	26.7	26.4	27.6	30.4	26.0	26.4	27.0	26.8	29.3	29.3	30.8	30.2
305	26.6	26.1	26.4	26.9	25.9	26.1	27.0	26.9	29.2	29.4	30.4	30.1
230	26.6	26.0	26.3	26.7	26.0	26.4	26.8	26.5	29.4	29.2	30.2	30.2
150	26.5	26.1	26.3	26.7	26.0	26.2	27.0	26.8	29.5	29.2	30.2	30.1
75	26.7	25.9	26.3	26.3	25.9	26.1	26.9	26.3	29.2	28.9	30.0	29.7
bottom	26.0	26.2	26.8	26.3	26.0	25.9	27.0	26.5	29.1	28.8	29.7	29.6

Table 17. Water temperatures, burns 5/31, 6/4, and 6/5

	Burn Number 5/31 17.2 m effective diameter				Burn Number 6/4 12.0 m effective diameter				Burn Number 6/5 17.2 m effective diameter			
	Time before ignition (s)		Time after extinction (s)		Time before ignition (s)		Time after extinction (s)		Time before ignition (s)		Time after extinction (s)	
	4280	3970	2030	NA	12590	12150	530	860	6670	6390	420	810
	Position				Position				Position			
	Center of west side of pan	SE corner of pan	NE corner of burn area	SE corner of pan	SW corner of burn area	SE corner of pan	SW corner of burn area	SE corner of pan	NW corner of pan	SE corner of pan	Center of west side of pan	NE corner of pan
Elevation (mm)	**Water temperature (°C)**				**Water temperature (°C)**				**Water temperature (°C)**			
surface (elevation mm)	27.2 (495)	27.4 (485)	53.8 (510)	47.1 (510)	27.6 (510)	27.6 (495)	48.0 (495)	35.8 (485)	27.3 (495)	27.7 (495)	58.0 (510)	44.0 (470)
460	27.4	27.4	37.2	40.6	28.0	27.7	37.0	34.4	27.5	27.4	45.1	44.2
380	27.4	27.4	28.3	27.9	27.3	27.7	31.1	31.8	27.6	27.7	28.8	28.1
305	27.1	27.4	28.3	27.8	27.4	27.5	28.7	31.2	27.4	27.6	28.6	28.3
230	27.4	27.3	28.2	27.7	26.9	27.5	28.2	28.8	27.4	27.5	28.3	27.8
150	27.4	27.4	28.3	28.0	26.9	27.4	27.8	29.1	27.3	27.4	28.2	28.4
75	27.5	27.3	28.2	27.5	27.0	27.1	27.8	28.9	27.2	27.6	27.8	28.0
bottom	27.4	27.4	28.0	27.6	26.9	27.0	28.0	28.9	27.0	27.4	27.6	28.5

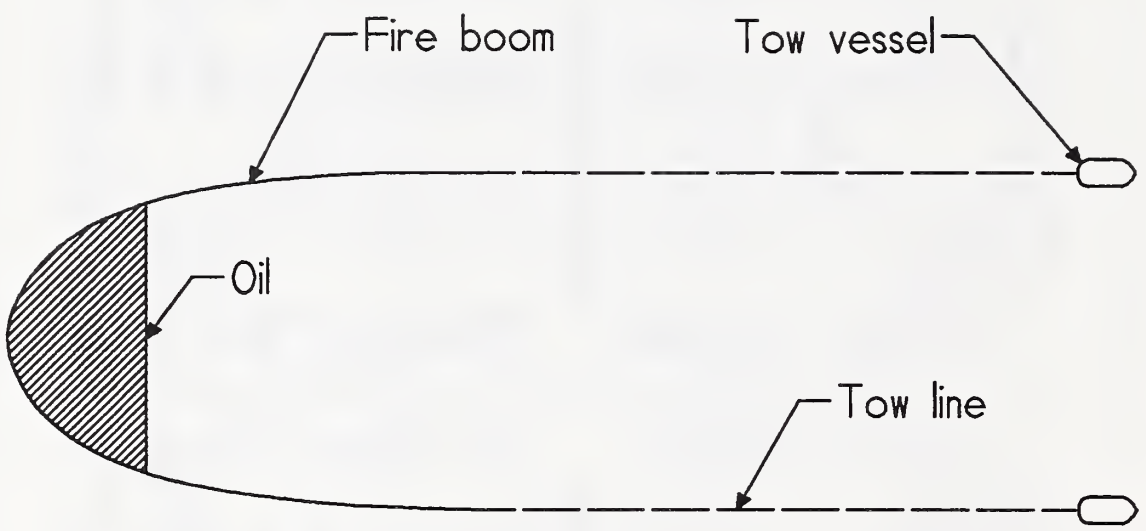

Figure 1. Schematic view of towed fire boom

Figure 2. USCG Safety and Fire Test Detachment mesoscale burn facility in Mobile, Alabama

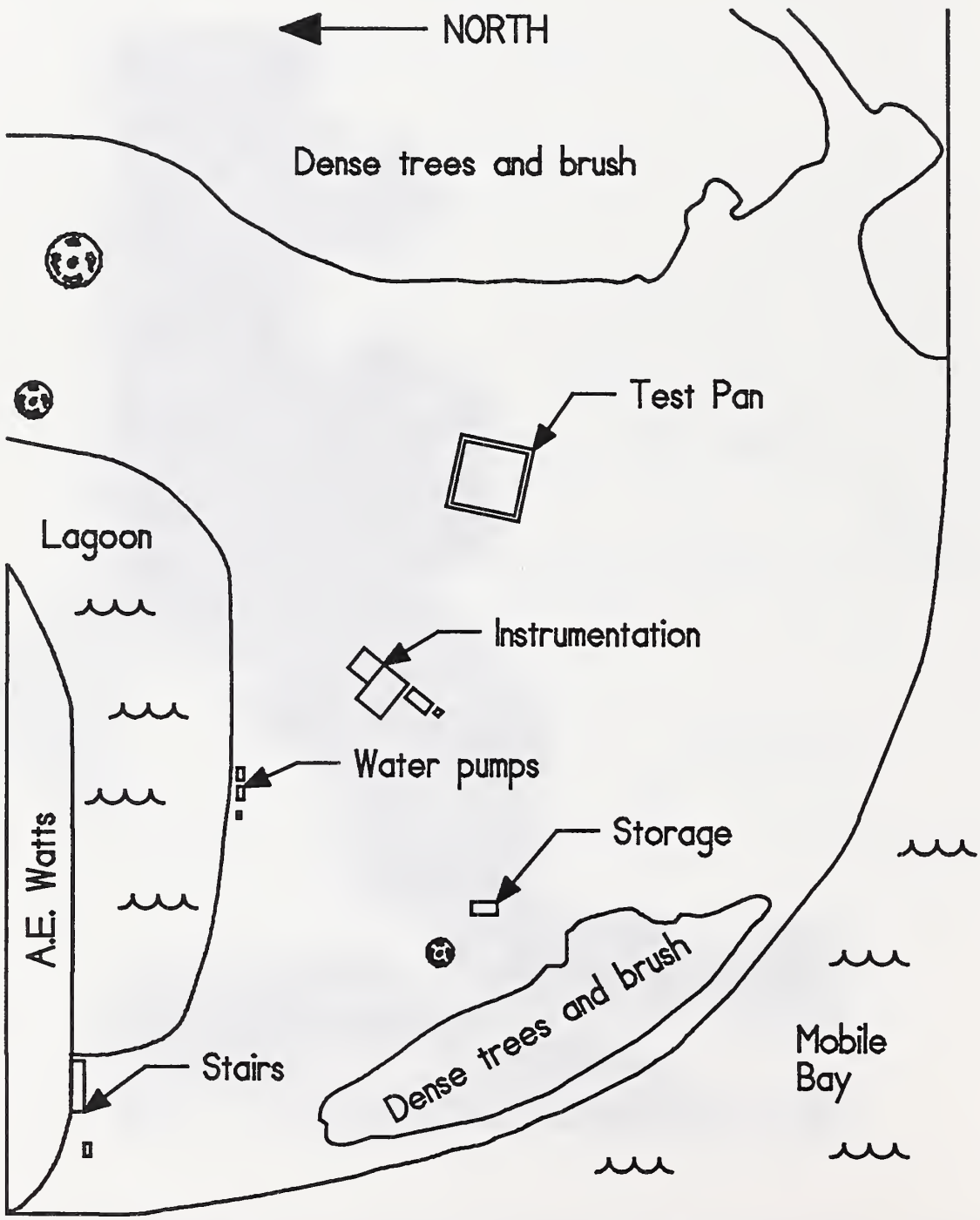

Figure 3. USCG mesoscale burn facility site plan

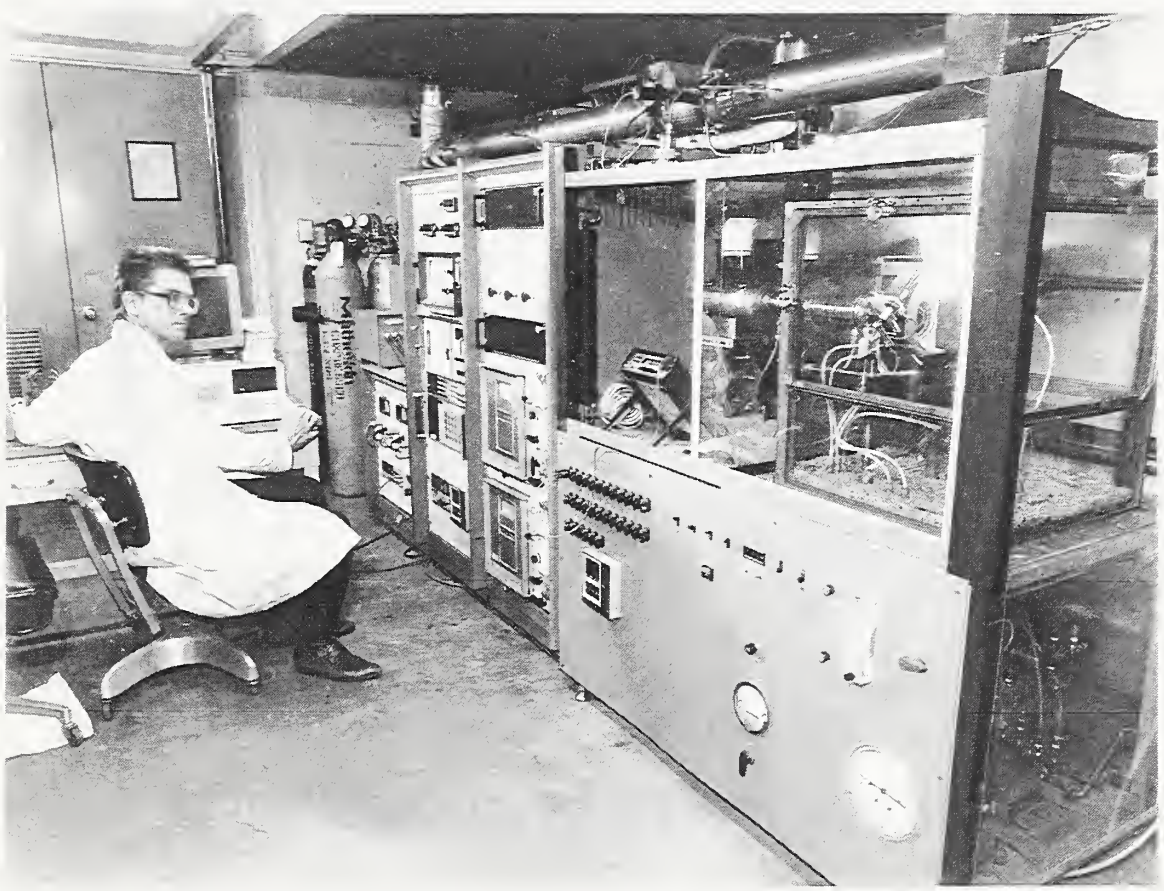

Figure 4. NIST Cone Calorimeter

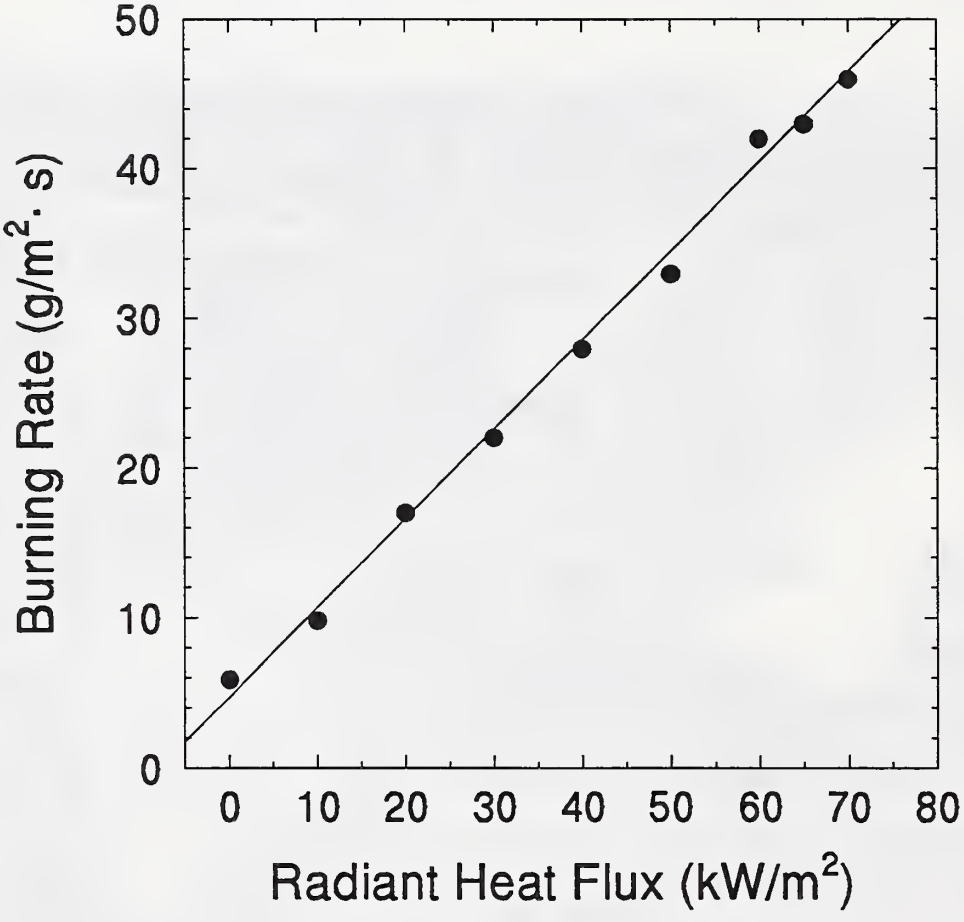

Figure 5. Heat of gasification

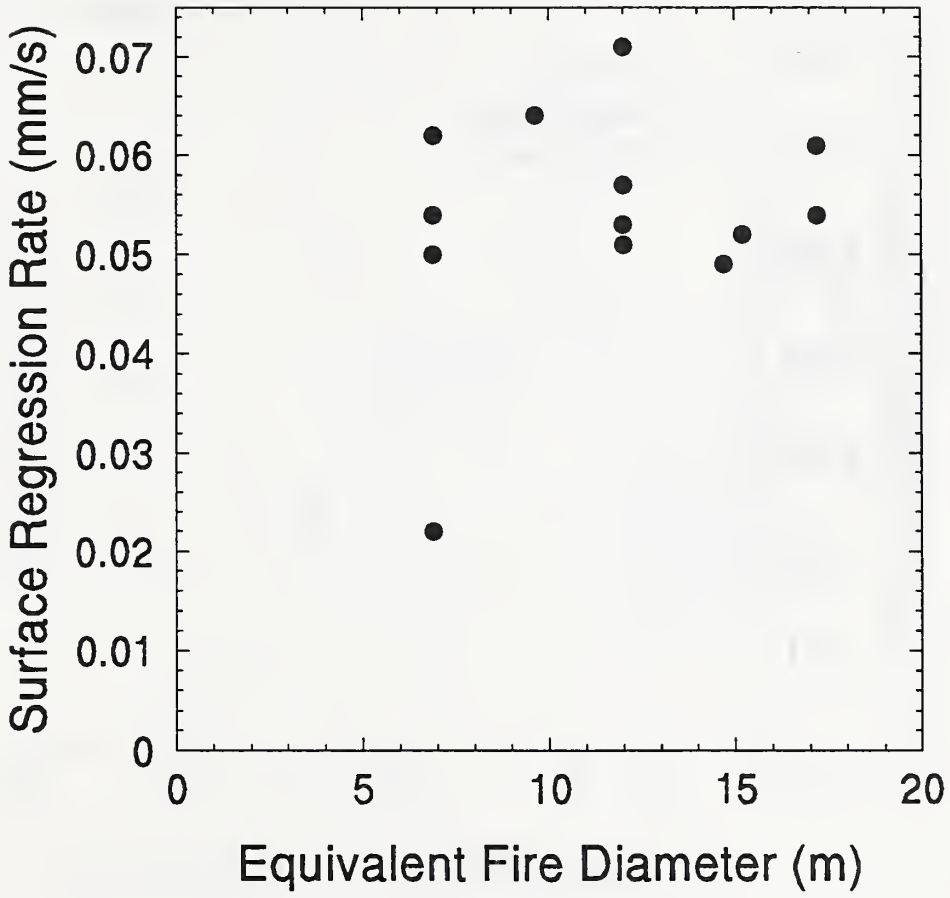

Figure 6. Average surface regression rate

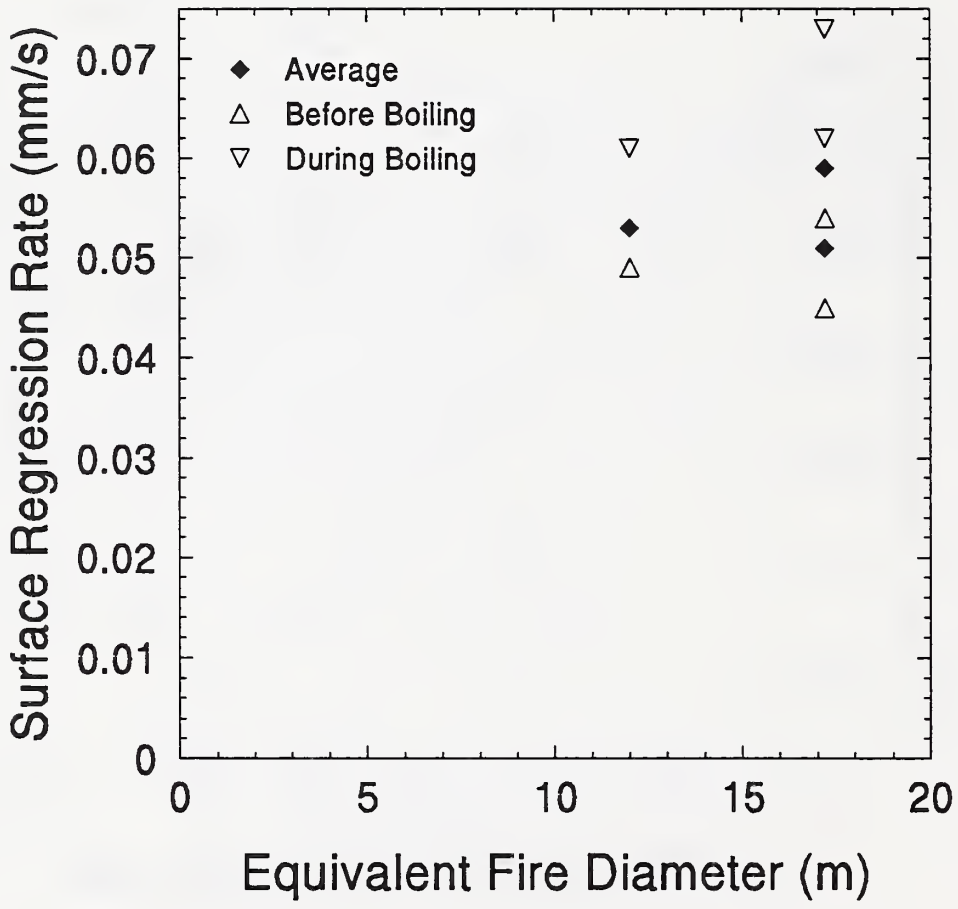

Figure 7. Average surface regression rate before and after boiling

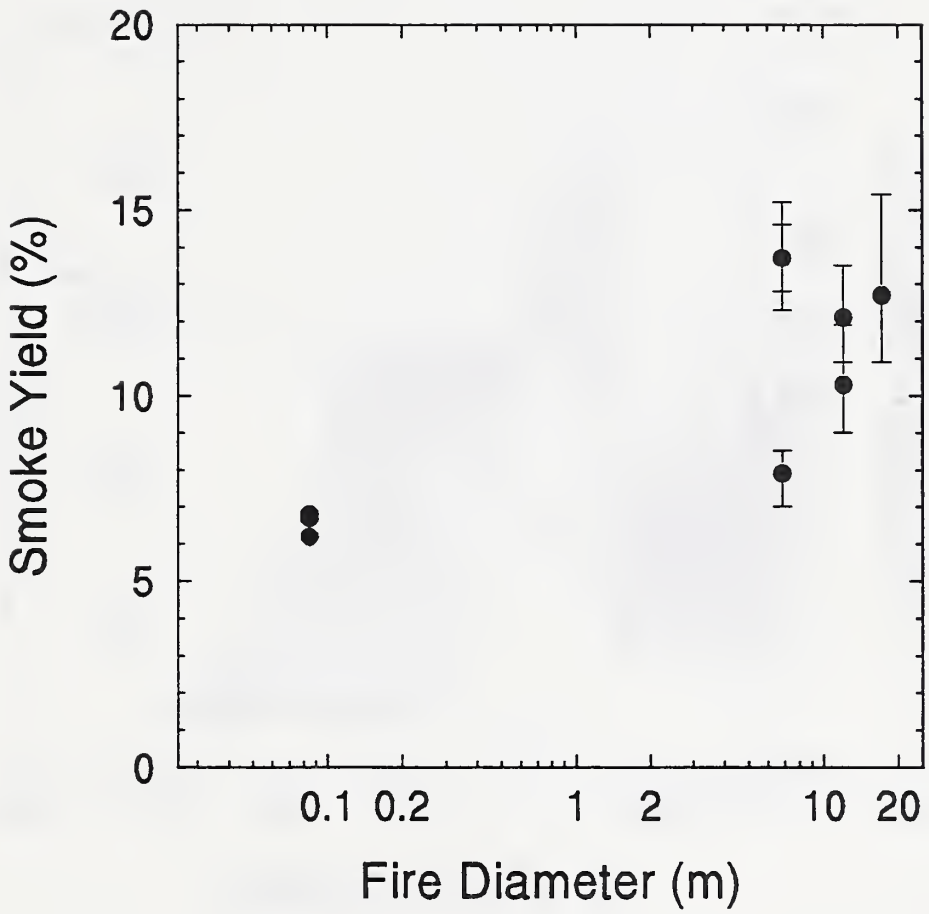

Figure 8. Smoke yield by carbon balance method (mesoscale and Cone Calorimeter)

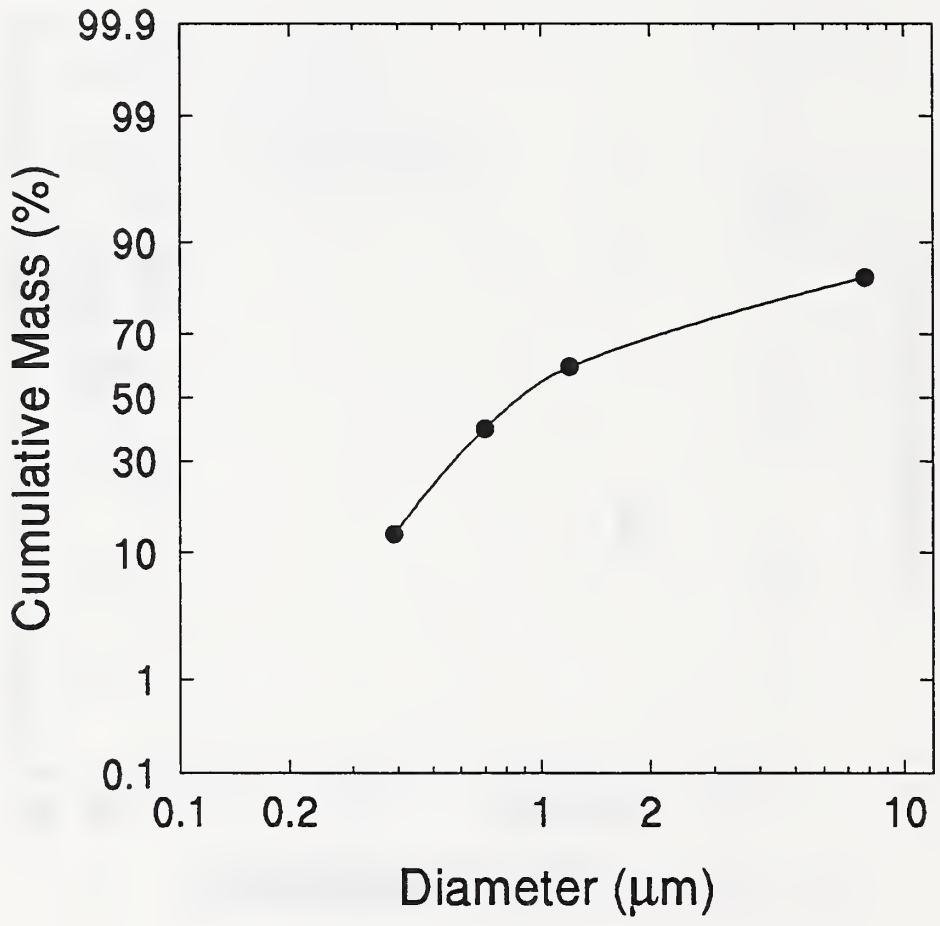

Figure 9. Size distribution of smoke particulate for burn 6/4

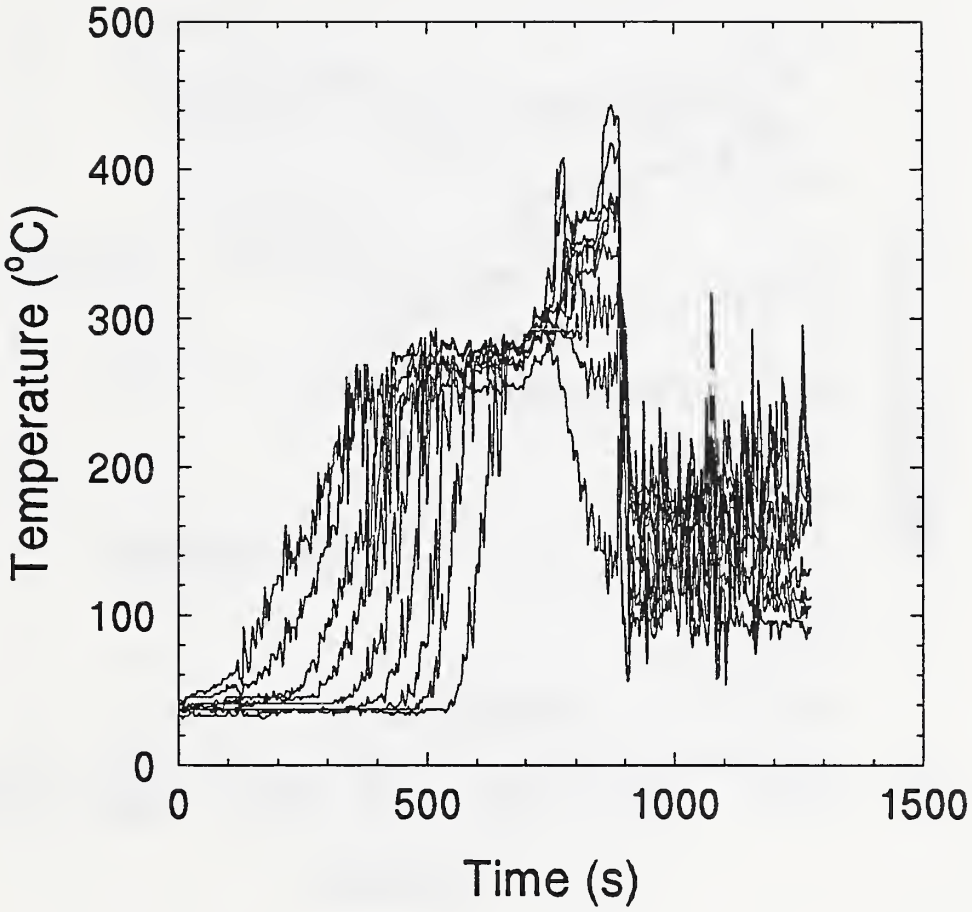

Figure 10. Oil/water temperatures for burn 5/17

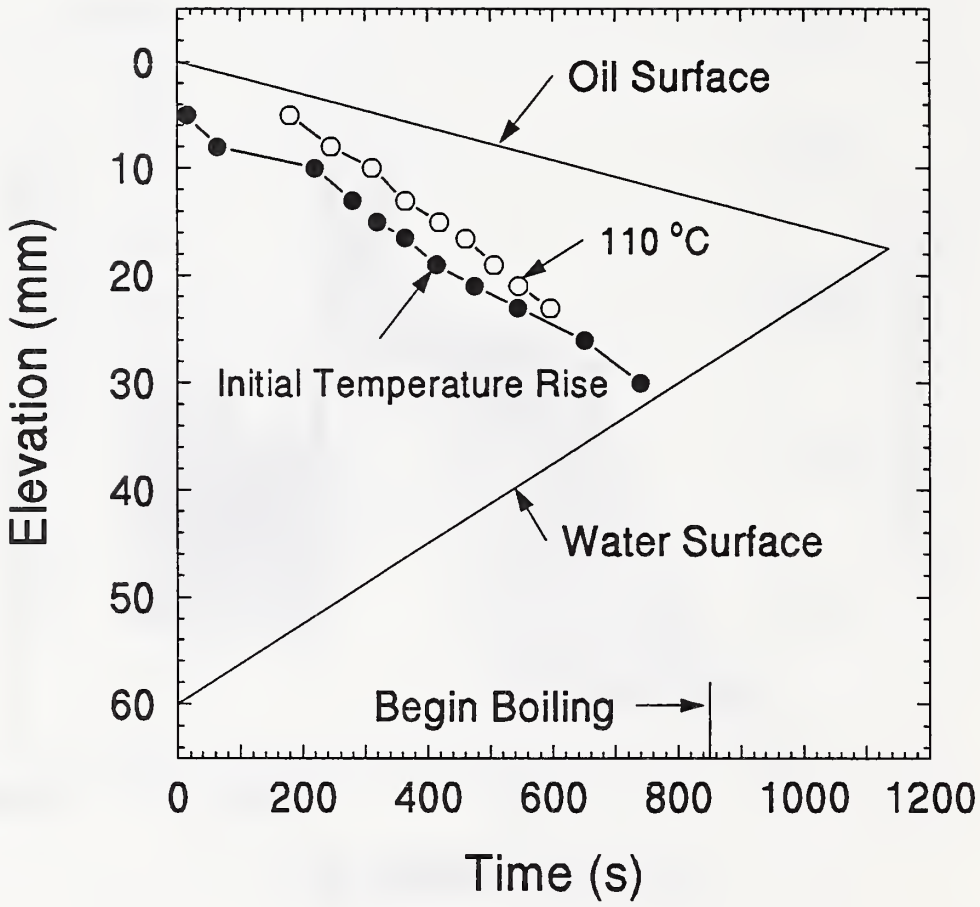

Figure 11. Thermal penetration for burn 5/17

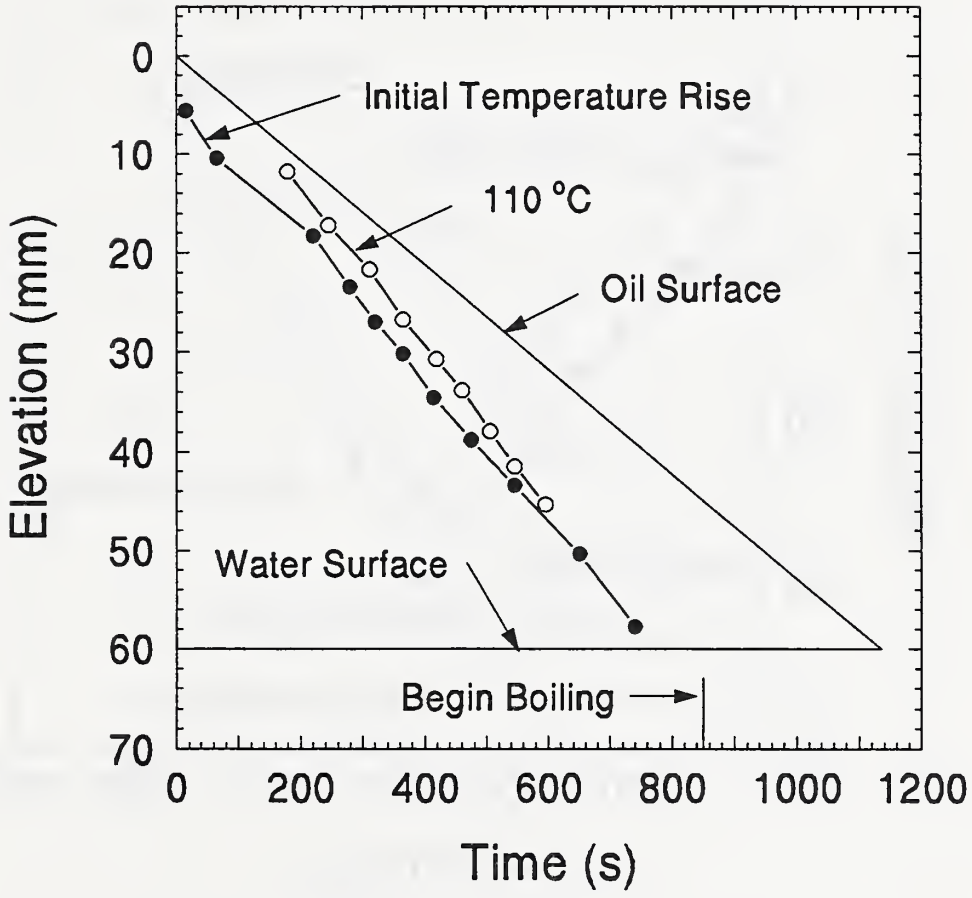

Figure 12. Thermal penetration relative to the water surface for burn 5/17

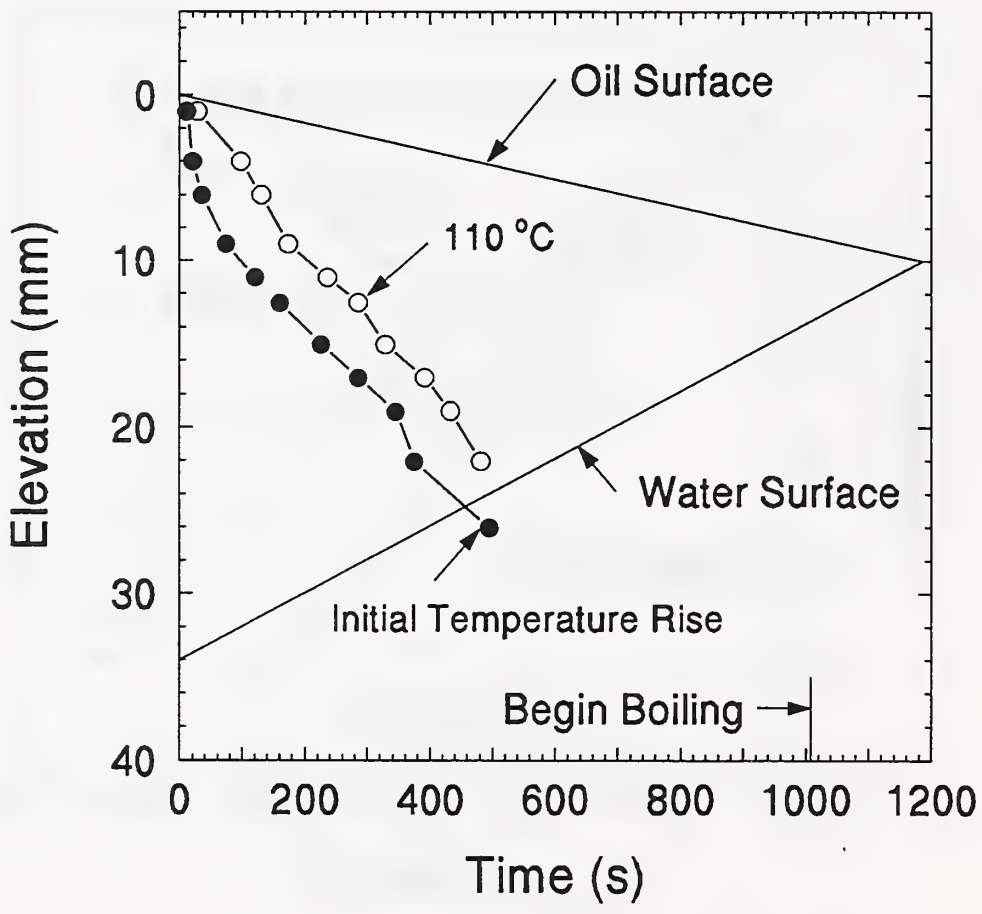

Figure 13. Thermal penetration for burn 5/16

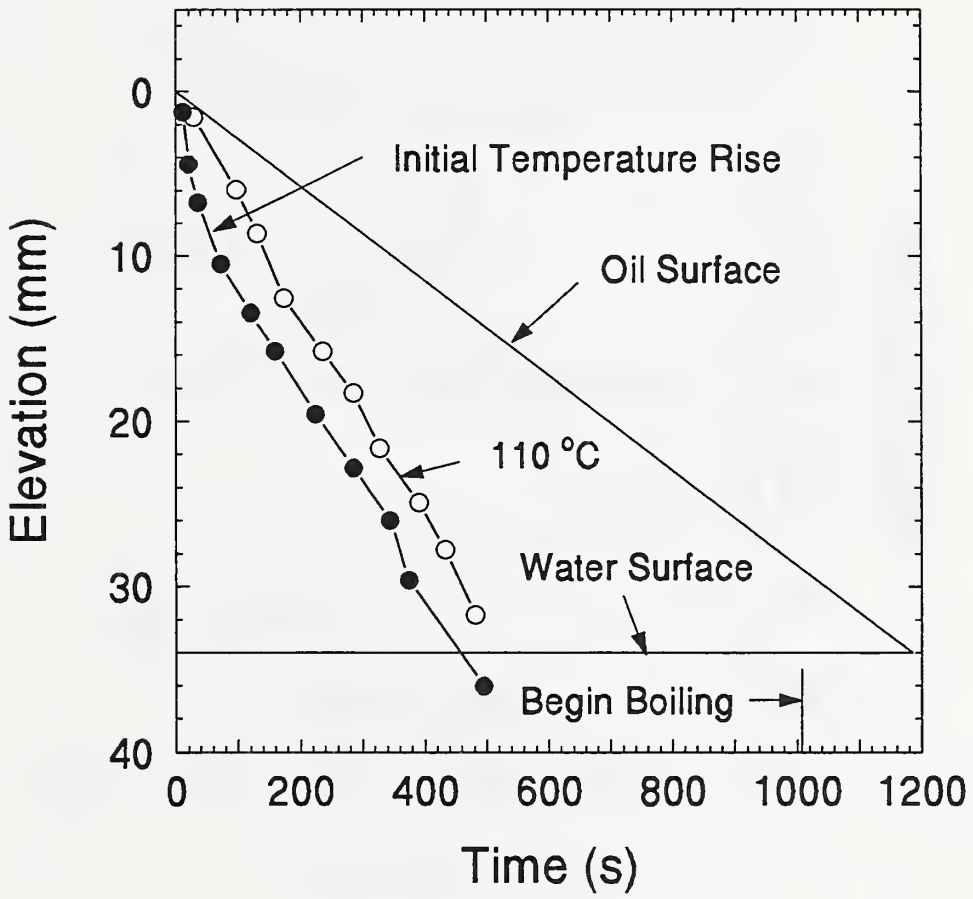

Figure 14. Thermal penetration relative to the water surface for burn 5/16

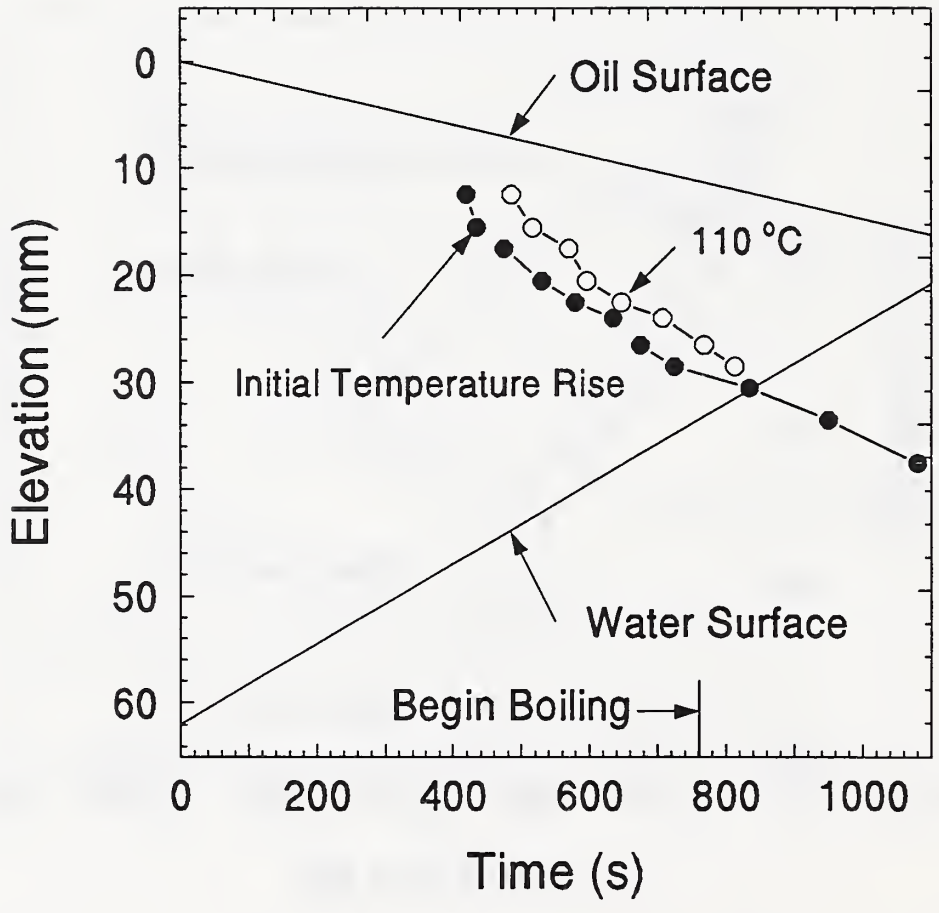

Figure 15. Thermal penetration for burn 5/29

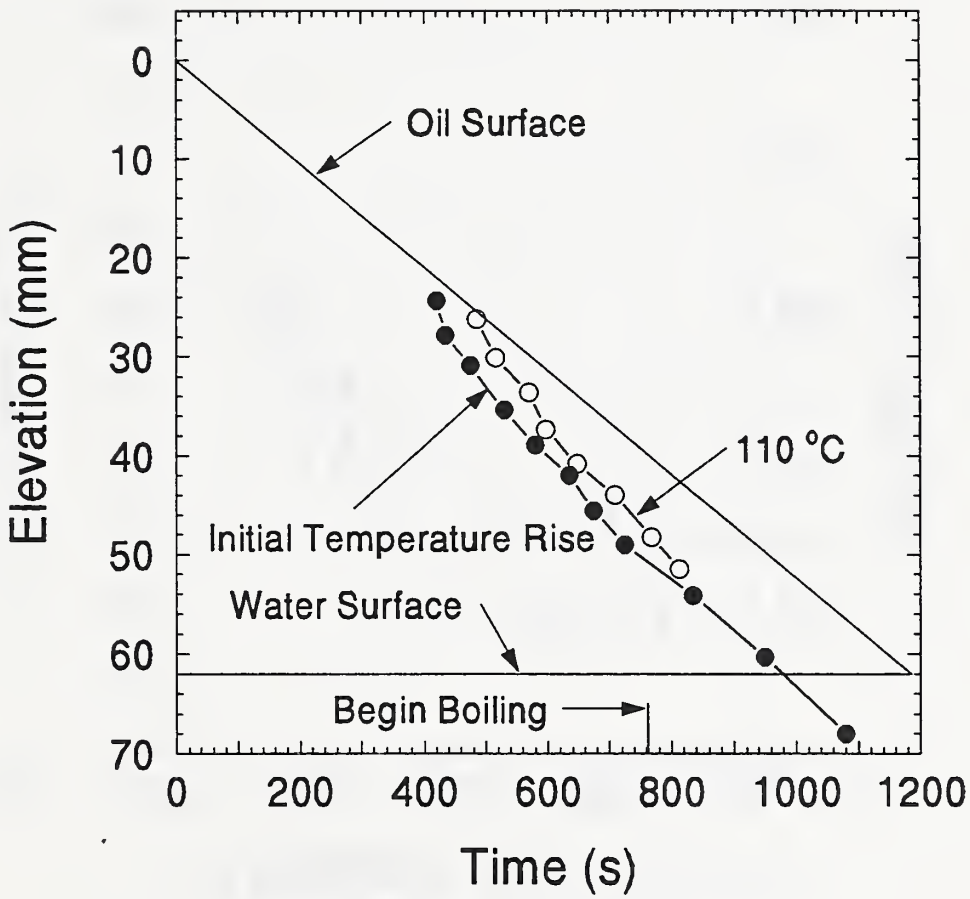

Figure 16. Thermal penetration relative to the water surface for burn 5/29

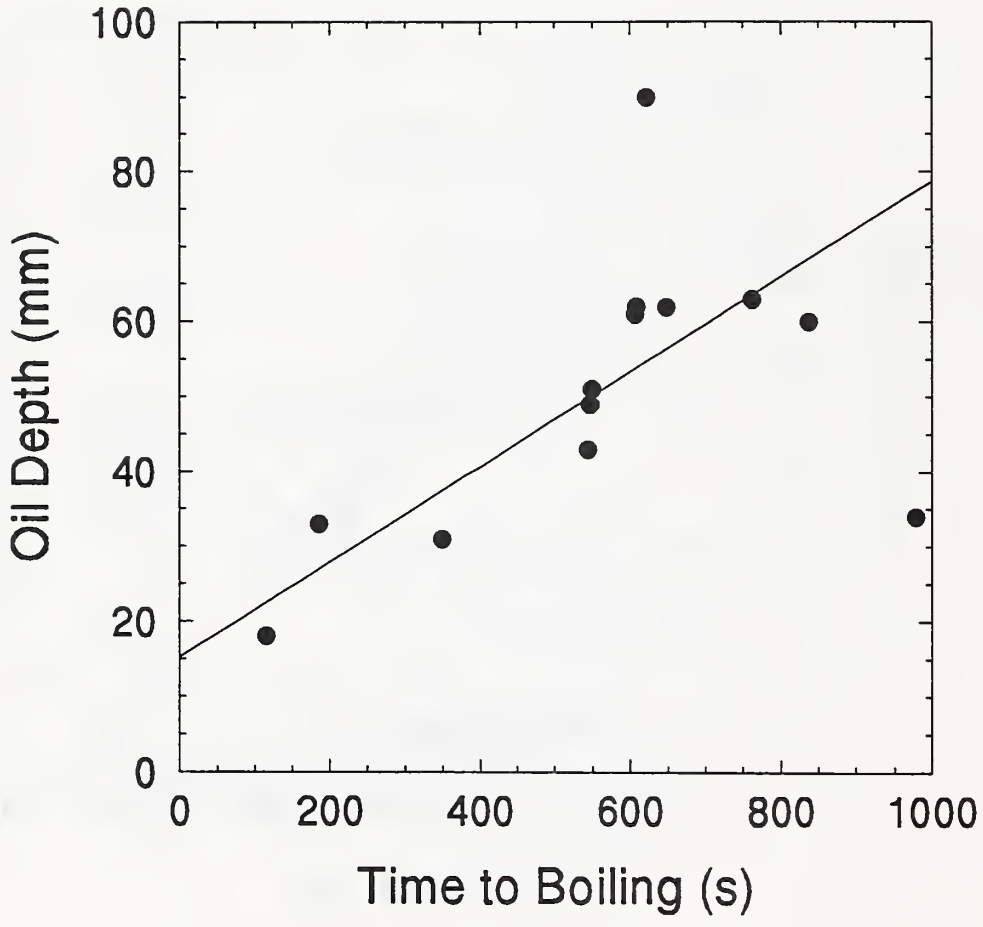

Figure 17. Time to boiling

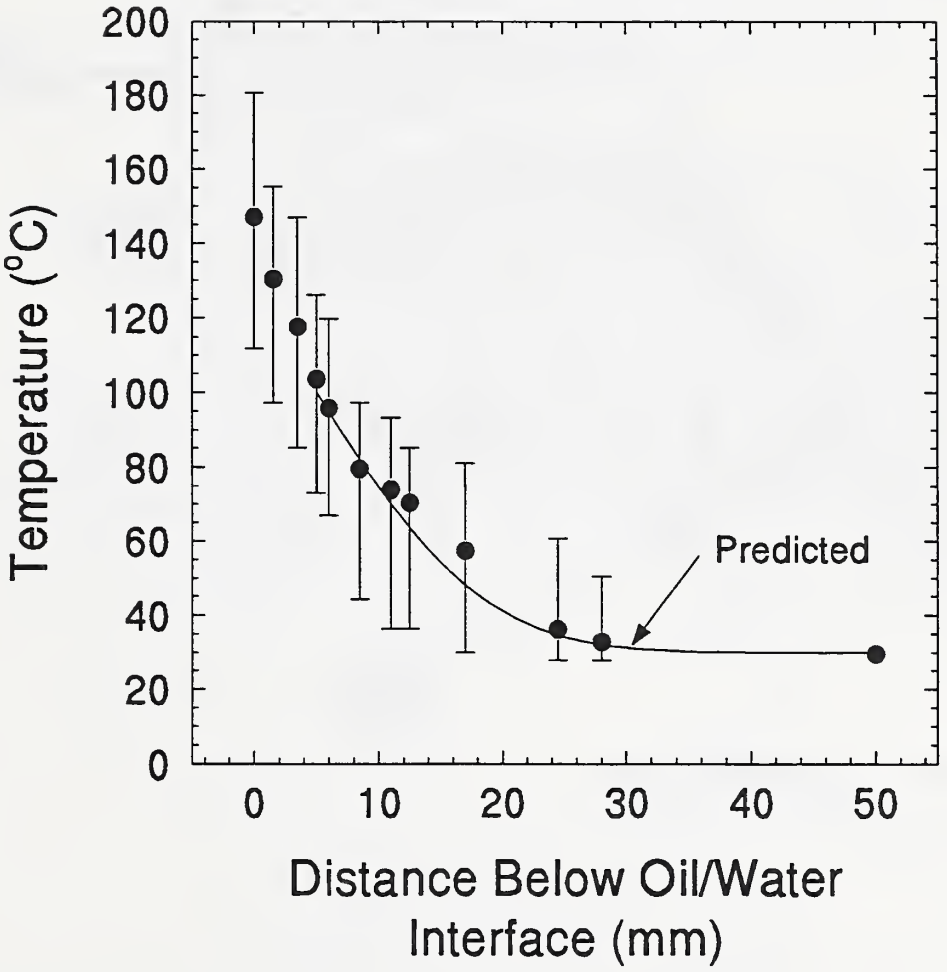

Figure 18. Water temperature profile at the begining of extinction for burn 5/31

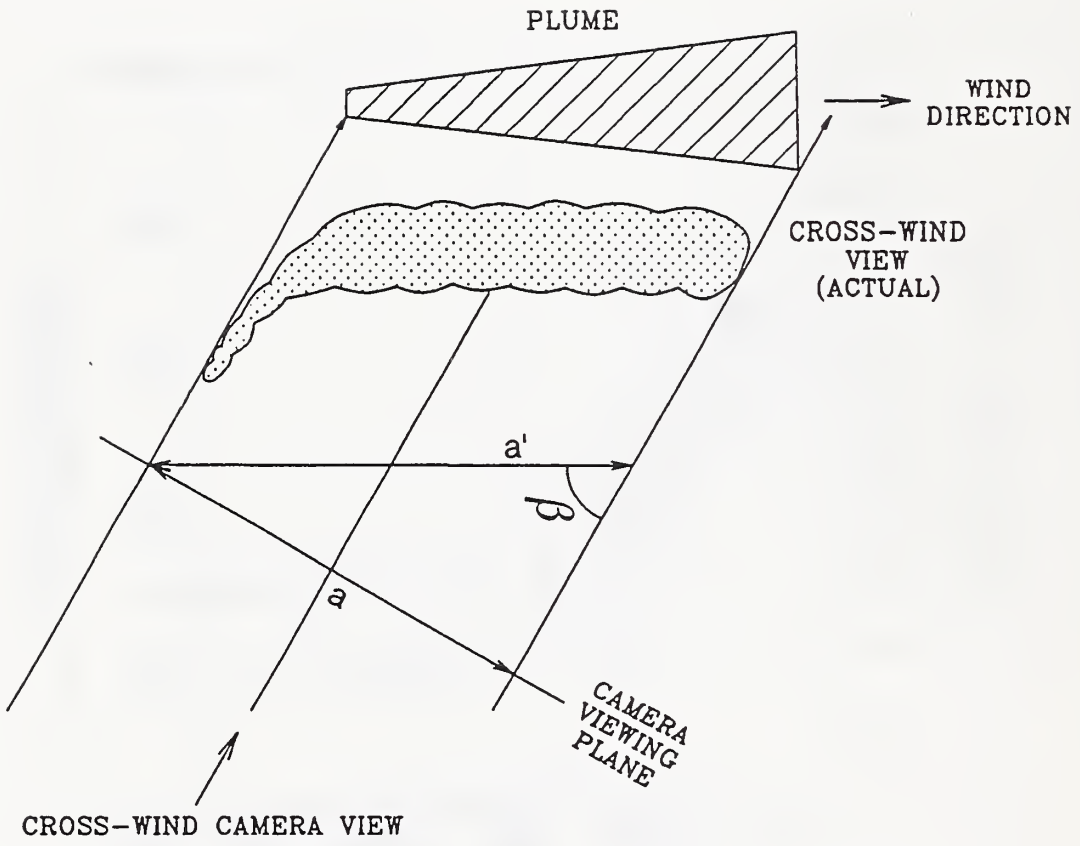

Figure 19. Geometric correction for plume length when observed from an oblique angle

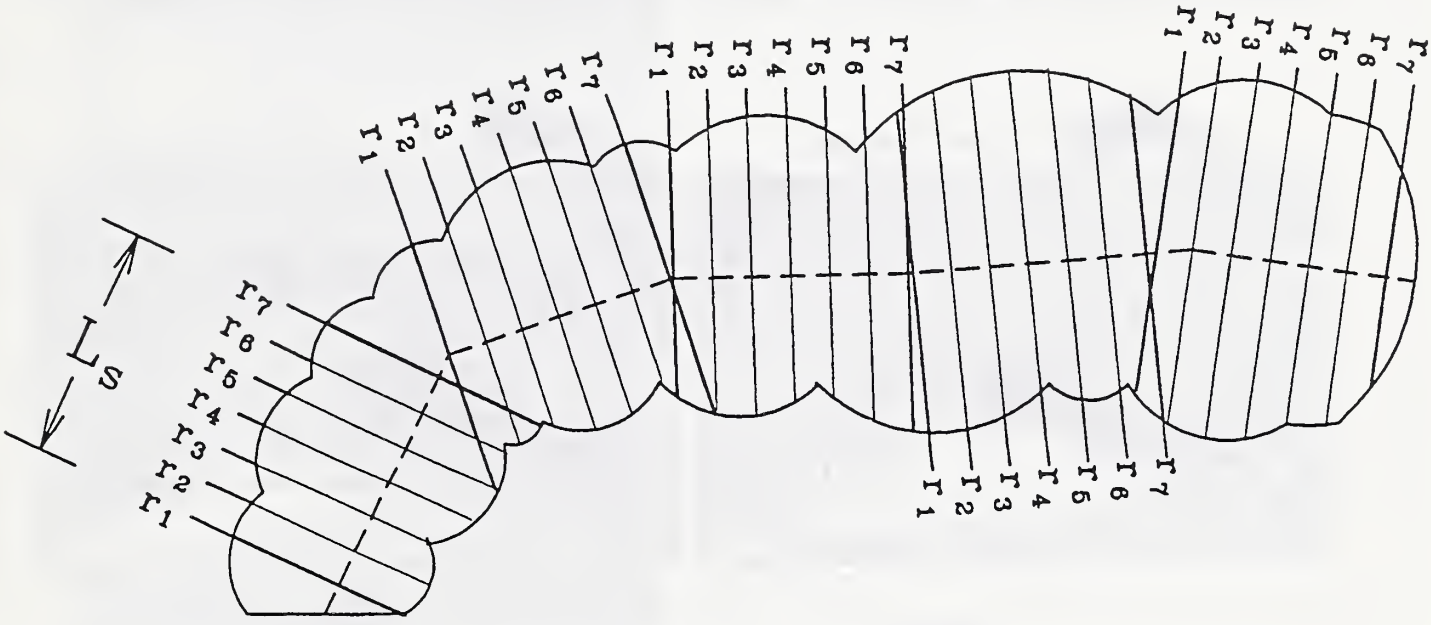

Figure 20. Segments used to calculate plume volume

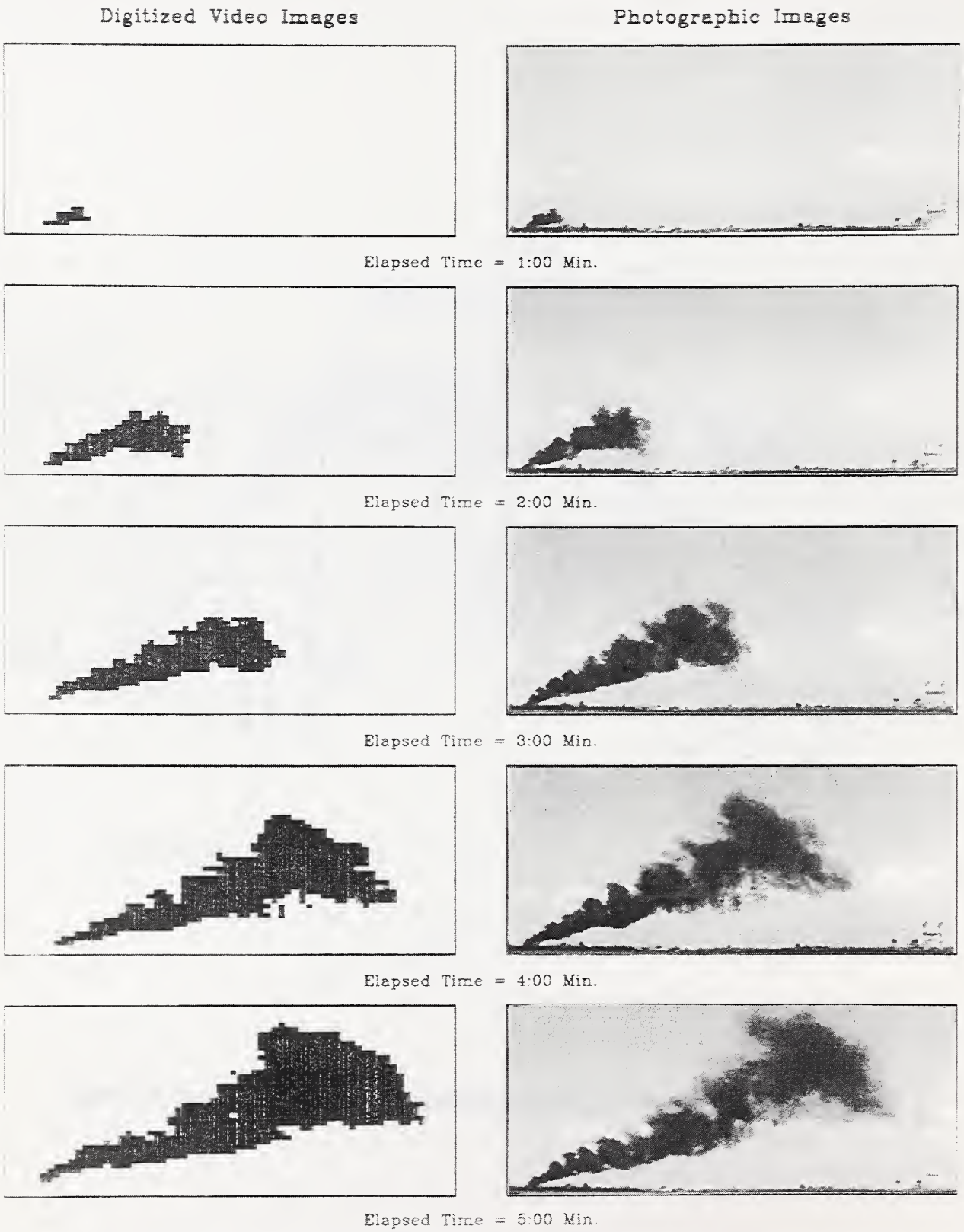

Figure 21. Plume photographs and corresponding digitized images for burn 5/30

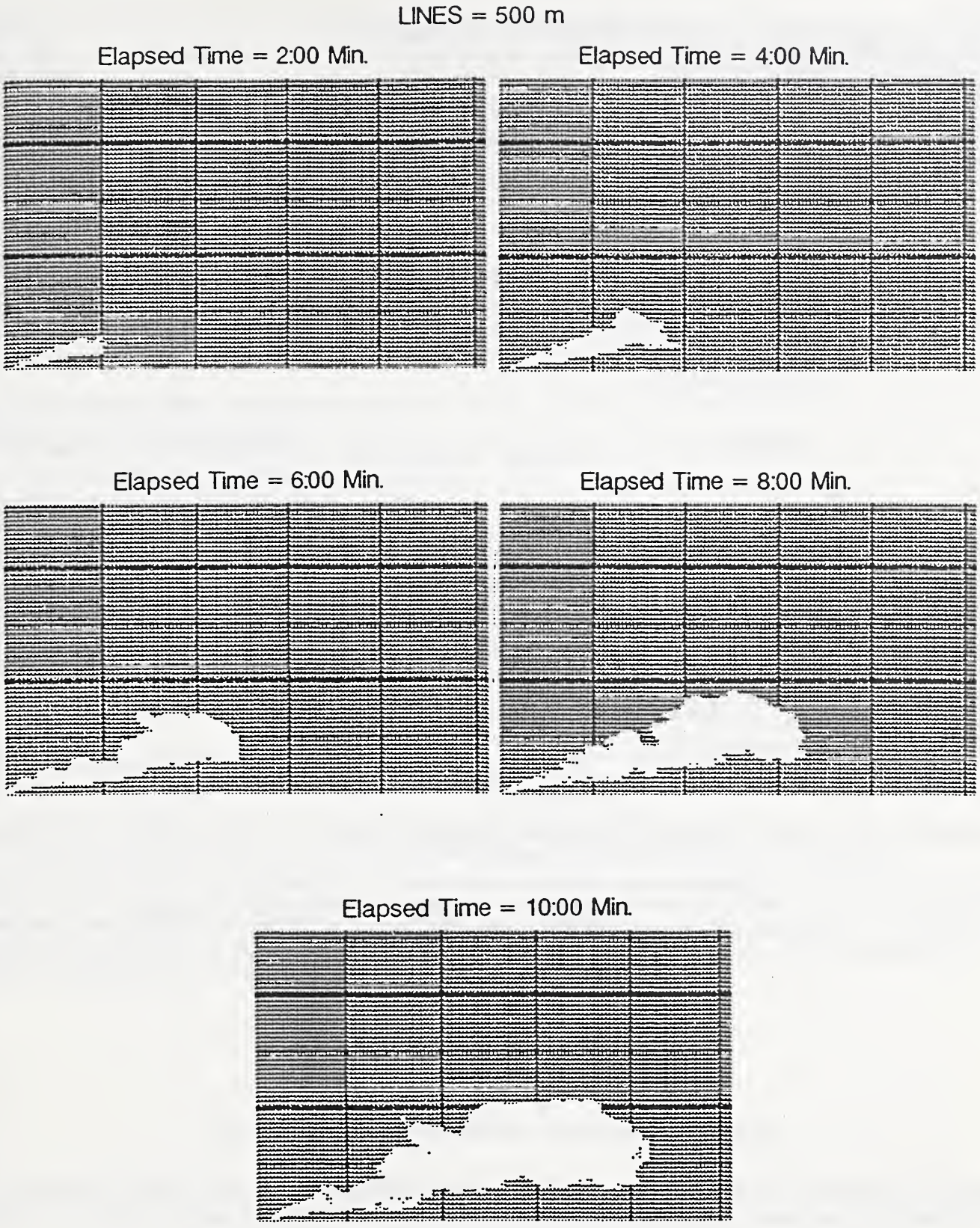

Figure 22. Digital images used in analysis of burn 5/30

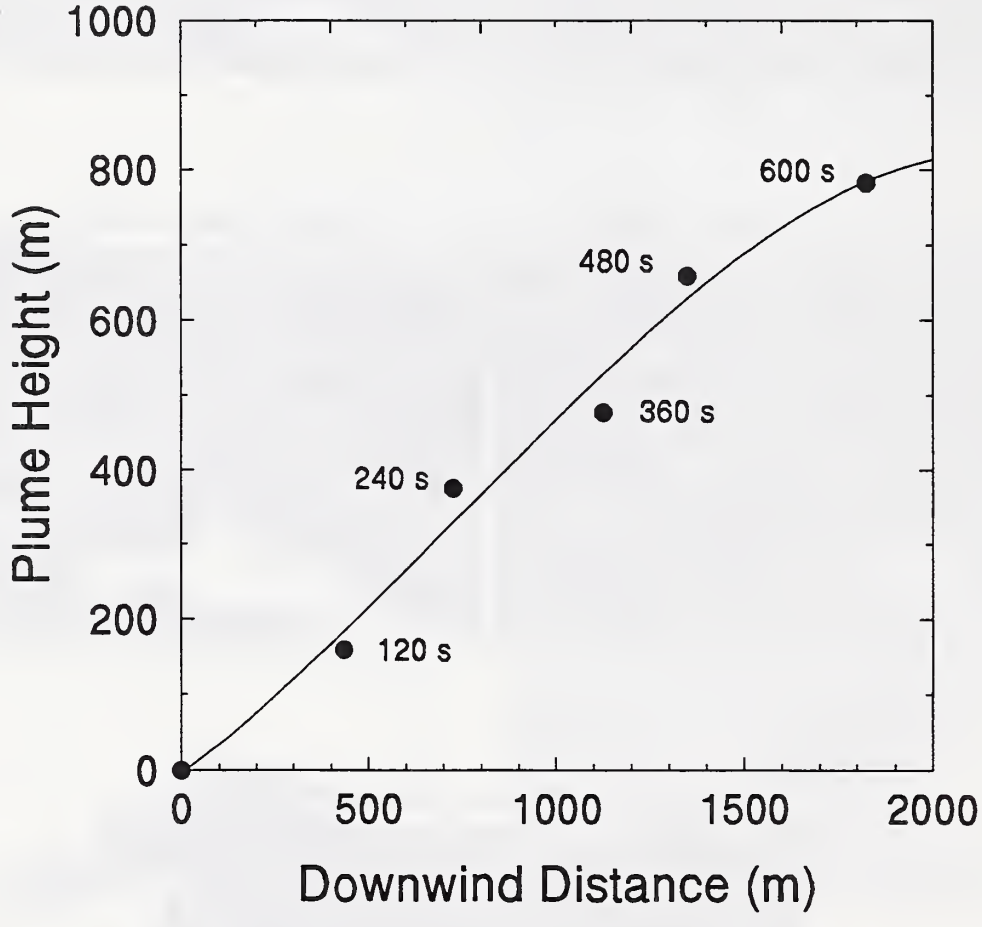

Figure 23. Plume height vs downwind distance for burn 5/30

NIST-114
(REV. 6-93)
ADMAN 4.09

U.S. DEPARTMENT OF COMMERCE
NATIONAL INSTITUTE OF STANDARDS AND TECHNOLOGY

MANUSCRIPT REVIEW AND APPROVAL

(ERB USE ONLY)	
ERB CONTROL NUMBER	DIVISION
PUBLICATION REPORT NUMBER	CATEGORY CODE
PUBLICATION DATE	NUMBER PRINTED PAGES

INSTRUCTIONS: ATTACH ORIGINAL OF THIS FORM TO ONE (1) COPY OF MANUSCRIPT AND SEND TO THE SECRETARY, APPROPRIATE EDITORIAL REVIEW BOARD

TITLE AND SUBTITLE (CITE IN FULL)

In Situ Burning of Oil Spills: Mesoscale Experiments

CONTRACT OR GRANT NUMBER

TYPE OF REPORT AND/OR PERIOD COVERED

AUTHOR(S) (LAST NAME, FIRST INITIAL, SECOND INITIAL)

Walton, W.D.

PERFORMING ORGANIZATION (CHECK (X) ONE BOX)

[X] NIST/GAITHERSBURG
[ ] NIST/BOULDER
[ ] JILA/BOULDER

LABORATORY AND DIVISION NAMES (FIRST NIST AUTHOR ONLY)

Building and Fire Research Laboratory

SPONSORING ORGANIZATION NAME AND COMPLETE ADDRESS (STREET, CITY, STATE, ZIP)

U.S. Department of Interior, Minerals Management Service
Technology Assessment and Research Branch
Herndon, VA 22070

PROPOSED FOR NIST PUBLICATION

[ ]	JOURNAL OF RESEARCH (NIST JRES)	[ ]	MONOGRAPH (NIST MN)	[ ]	LETTER CIRCULAR
[ ]	J. PHYS. & CHEM. REF. DATA (JPCRD)	[ ]	NATL. STD. REF. DATA SERIES (NIST NSRDS)	[ ]	BUILDING SCIENCE SERIES
[ ]	HANDBOOK (NIST HB)	[ ]	FEDERAL INF. PROCESS. STDS. (NIST FIPS)	[ ]	PRODUCT STANDARDS
[ ]	SPECIAL PUBLICATION (NIST SP)	[ ]	LIST OF PUBLICATIONS (NIST LP)	[ ]	OTHER _____
[ ]	TECHNICAL NOTE (NIST TN)	[X]	NIST INTERAGENCY/INTERNAL REPORT (NISTIR)		

PROPOSED FOR NON-NIST PUBLICATION (CITE FULLY) [ ] U.S. [ ] FOREIGN

PUBLISHING MEDIUM

[X] PAPER [ ] CD-ROM
[ ] DISKETTE (SPECIFY) _____
[ ] OTHER (SPECIFY)

SUPPLEMENTARY NOTES

ABSTRACT (A 2000-CHARACTER OR LESS FACTUAL SUMMARY OF MOST SIGNIFICANT INFORMATION. IF DOCUMENT INCLUDES A SIGNIFICANT BIBLIOGRAPHY OR LITERATURE SURVEY, CITE IT HERE. SPELL OUT ACRONYMS ON FIRST REFERENCE.) (CONTINUE ON SEPARATE PAGE, IF NECESSARY.)

In 1991 a series of 14 mesoscale fire experiments were performed to measure the burning characteristics of crude oil on salt water. These oil burns in a pan ranged in size from 6 m square to 15 m square. Results of the measurements for burning rate, oil temperature, water temperature, smoke particle size distribution, smoke plume trajectory, and smoke particulate yield are provided. The burning rate as indicated by the regression rate of the oil surface was found to be 0.055 ± 0.01 mm/s and smoke particulate yields were found to be approximately 0.13 of the oil burned on a mass basis.

KEY WORDS (MAXIMUM OF 9; 28 CHARACTERS AND SPACES EACH; SEPARATE WITH SEMICOLONS; ALPHABETIC ORDER; CAPITALIZE ONLY PROPER NAMES)

burning rate, crude oil, fire research, fire tests, heat release rate, oil spills, particle size distribution, plumes, pool fires, smoke yield

AVAILABILITY

[X] UNLIMITED [ ] FOR OFFICIAL DISTRIBUTION - DO NOT RELEASE TO NTIS
[ ] ORDER FROM SUPERINTENDENT OF DOCUMENTS, U.S. GPO, WASHINGTON, DC 20402
[X] ORDER FROM NTIS, SPRINGFIELD, VA 22161

NOTE TO AUTHOR(S): IF YOU DO NOT WISH THIS MANUSCRIPT ANNOUNCED BEFORE PUBLICATION, PLEASE CHECK HERE. [ ]

WORDPERFECT